

Research



Cite this article: Albee LJ, LaPorte HM, Gao X, Eby JM, Cheng Y-H, Nevins AM, Volkman BF, Gaponenko V, Majetschak M. 2018 Identification and functional characterization of arginine vasopressin receptor 1A : atypical chemokine receptor 3 heteromers in vascular smooth muscle. *Open Biol.* **8**: 170207. <http://dx.doi.org/10.1098/rsob.170207>

Received: 30 August 2017

Accepted: 8 January 2018

Subject Area:

biochemistry/cellular biology/immunology/
molecular biology

Keywords:

vasoconstriction, vasopressor, arginine
vasopressin, CXCL11, CXCL12, ubiquitin

Author for correspondence:

Matthias Majetschak

e-mail: mmajetschak@luc.edu

Identification and functional characterization of arginine vasopressin receptor 1A : atypical chemokine receptor 3 heteromers in vascular smooth muscle

Lauren J. Albee¹, Heather M. LaPorte¹, Xianlong Gao¹, Jonathan M. Eby¹, You-Hong Cheng¹, Amanda M. Nevins³, Brian F. Volkman³, Vadim Gaponenko⁴ and Matthias Majetschak^{1,2}

¹Burn and Shock Trauma Research Institute, Department of Surgery, and ²Department of Molecular Pharmacology and Therapeutics, Loyola University Chicago Stritch School of Medicine, 2160 S. 1st Avenue, Maywood, IL 60153, USA

³Department of Biochemistry, Medical College of Wisconsin, Milwaukee, WI 53226, USA

⁴Department of Biochemistry and Molecular Genetics, University of Illinois at Chicago, Chicago, IL 60607, USA

MM, 0000-0002-4086-0887

Recent observations suggest that atypical chemokine receptor (ACKR)3 and chemokine (C-X-C motif) receptor (CXCR)4 regulate human vascular smooth muscle function through hetero-oligomerization with α_1 -adrenoceptors. Here, we show that ACKR3 also regulates arginine vasopressin receptor (AVPR)1A. We observed that ACKR3 agonists inhibit arginine vasopressin (aVP)-induced inositol trisphosphate (IP₃) production in human vascular smooth muscle cells (hVSMCs) and antagonize aVP-mediated constriction of isolated arteries. Proximity ligation assays, co-immunoprecipitation and bioluminescence resonance energy transfer experiments suggested that recombinant and endogenous ACKR3 and AVPR1A interact on the cell surface. Interference with ACKR3 : AVPR1A heteromerization using siRNA and peptide analogues of transmembrane domains of ACKR3 abolished aVP-induced IP₃ production. aVP stimulation resulted in β -arrestin 2 recruitment to AVPR1A and ACKR3. While ACKR3 activation failed to cross-recruit β -arrestin 2 to AVPR1A, the presence of ACKR3 reduced the efficacy of aVP-induced β -arrestin 2 recruitment to AVPR1A. AVPR1A and ACKR3 co-internalized upon agonist stimulation in hVSMC. These data suggest that AVPR1A : ACKR3 heteromers are constitutively expressed in hVSMC, provide insights into molecular events at the heteromeric receptor complex, and offer a mechanistic basis for interactions between the innate immune and vasoactive neurohormonal systems. Our findings suggest that ACKR3 is a regulator of vascular smooth muscle function and a possible drug target in diseases associated with impaired vascular reactivity.

1. Background

The 7-transmembrane domain (TM) receptors chemokine (C-X-C motif) receptor 4 (CXCR4) and atypical chemokine receptor 3 (ACKR3) are involved in the regulation of vascular function and blood pressure control [1–7]. The underlying mechanisms, however, are not well understood. While CXCR4 is a typical G protein-coupled receptor (GPCR) that couples to $G\alpha_i$ and recruits β -arrestin, ACKR3 does not couple to G proteins but recruits β -arrestin, leading to receptor internalization and G protein-independent signalling events [8,9]. Both receptors share C-X-C chemokine ligand 12 (CXCL12, stromal cell-derived factor 1) as a cognate agonist [8]. Furthermore, CXCR4 and ACKR3 are thought to form heteromeric complexes, resulting in preferential activation of β -arrestin signalling over

canonical G protein signalling pathways upon activation with CXCL12 [10,11]. Besides heteromerization with ACKR3, CXCR4 may form heteromeric complexes with multiple other GPCRs, such as chemokine (C-C motif) receptor (CCR)2, CCR5, CXCR3, chemerin receptor 23, β_2 -adrenergic receptor (AR), δ -opioid receptor or cannabinoid receptor 2, leading to altered pharmacological properties of the interacting receptor partners [11–18].

Recently, we reported cross-talk between CXCR4, ACKR3 and α_1 -ARs in vascular smooth muscle, through which activation of the chemokine receptors regulates α_1 -AR-mediated vasoconstriction with diametrically opposing effects; while CXCR4 activation enhanced, ACKR3 activation attenuated α_1 -AR-induced vasoconstriction [7]. Subsequently, we provided evidence that α_{1A} -AR preferentially forms heteromeric complexes with CXCR4 and ACKR3 protomers/homodimers, whereas $\alpha_{1B/D}$ -AR hetero-oligomerizes with the CXCR4:ACKR3 heteromer, which appears to be essential for $\alpha_{1B/D}$ -AR signalling and function in human vascular smooth muscle cells (hVSMCs) [19–21]. Furthermore, we have shown that simultaneous blockade of CXCR4 and activation of ACKR3 with the synthetic ligand TC14012 result in vasodilatory shock and cardiovascular collapse in normal animals [7]. It appears unlikely, however, that these effects can be attributed exclusively to ACKR3-mediated inhibition of α_1 -AR in vascular smooth muscle, thus suggesting additional interactions between ACKR3 and the vasoactive neurohormonal system. Because interactions between CXCL12 and arginine vasopressin (aVP) have previously been observed in the central nervous system [22,23], we tested whether aVP receptors (AVPRs) cross-talk with ACKR3 and/or CXCR4 in the regulation of intrinsic vascular smooth muscle function. Here, we provide evidence that ACKR3 also regulates AVPR1A signalling and function in VSMC via formation of heteromeric receptor complexes. We show that heteromerization between AVPR1A and ACKR3 facilitates AVPR1A-mediated G_{α_q} signalling and limits aVP-induced β -arrestin 2 recruitment to AVPR1A, and that activation of ACKR3 inhibits aVP-mediated signalling and vasoconstriction. These findings suggest that ACKR3 is a regulator of VSMC function, which controls endogenous and clinically important vasopressor actions.

2. Results and discussion

2.1. Activation of ACKR3 antagonizes aVP-mediated G_{α_q} signalling and function in vascular smooth muscle

We used pressure myography to assess whether CXCR4 and/or ACKR3 activation influence aVP-induced constriction of isolated mesenteric resistance arteries. α_1 -AR-induced vasoconstriction upon phenylephrine (PE) stimulation was used as a positive control. In agreement with our previous observations [7], the ACKR3 and CXCR3 agonist CXCL11 antagonized PE-induced vasoconstriction, whereas the CXCR4 agonist ubiquitin, which does not bind to ACKR3 [24], enhanced PE-induced vasoconstriction (figure 1a). While ubiquitin did not affect aVP-induced vasoconstriction, CXCL11 also antagonized vasoconstriction upon aVP stimulation (figure 1b). To confirm these effects of ACKR3 activation on aVP-induced vasoconstriction, we tested the effects of CXCL12, a CXCR4 and ACKR3

agonist, and of CXCL11 (3–73), an N-terminal truncated form of CXCL11 lacking amino acids 1 and 2, which has been described to show significantly reduced biological activity, when compared with wild-type CXCL11 [25,26]. To compare ACKR3 activity of these ligands, we first measured β -arrestin 2 recruitment to ACKR3 upon ligand stimulation using the PRESTO-Tango cell system [27,28] (figure 1c). While the potency of CXCL12 to recruit β -arrestin 2 to ACKR3 was 2.2-fold higher (EC_{50} (95% confidence interval (CI)) 1.3 (0.8–2.1) nM) than that of CXCL11 (EC_{50} (95% CI) 2.9 (2.1–4.0) nM, $p < 0.01$), both agonists showed comparable efficacy for β -arrestin 2 recruitment to ACKR3. When compared with CXCL11 and CXCL12, potency and efficacy of CXCL11 (3–73) for β -arrestin 2 recruitment to ACKR3 were significantly reduced (EC_{50} (95% CI) 11 (4–240) nM, top plateau: $65 \pm 7\%$ relative luminescence (RLU), $p < 0.01$ for both versus CXCL11 and CXCL12). When tested in pressure myography experiments, CXCL11 and CXCL12 attenuated PE- and aVP-induced vasoconstriction to a similar degree ($p < 0.05$ for vehicle versus CXCL11 and CXCL12; $p > 0.05$ for CXCL11 versus CXCL12), whereas CXCL11 (3–73) did not (figure 1d,e). The previous findings that CXCL12 binds to ACKR3 with sevenfold to 20-fold higher affinity than CXCL11 are not contradictory to our observations, because maximal biological responses of other GPCRs have been observed at ligand occupancies of only a small fraction of receptors [29–32]. In addition, our findings are consistent with the recent observation that the potency of CXCL12 to induce β -arrestin recruitment to ACKR3 when measured in a bioluminescence resonance energy transfer (BRET)-based assay was twofold higher than that of CXCL11 [30]. The significantly reduced potency and efficacy of truncated CXCL11 (3–73) to activate ACKR3 signalling suggest that its weak agonist activity was insufficient to evoke the functional biological response in intact arteries that we observed with the native ACKR3 agonists.

To test whether the antagonizing effects of ACKR3 are accompanied by corresponding effects on AVPR-mediated G_{α_q} signalling, we measured inositol trisphosphate (IP_3) production in hVSMC upon aVP stimulation. As shown in figure 1f, CXCL11, CXCL12 and TC14012, a synthetic ACKR3 agonist and CXCR4 antagonist [33], inhibited aVP-induced IP_3 production. These data suggest that ACKR3 activation inhibits AVPR signalling and function in hVSMC.

2.2. ACKR3 forms heteromeric complexes with AVPR1A

We have shown previously that α_1 -ARs form hetero-oligomeric complexes with ACKR3 and CXCR4 in hVSMC, through which $\alpha_{1B/D}$ -AR signalling and function are regulated [19–21]. Thus, we tested whether CXCR4 and ACKR3 may also form hetero-oligomeric complexes with AVPR1A, the receptor subtype which is responsible for the vasopressor action of aVP in VSMC [34]. We first co-expressed recombinant FLAG-tagged CXCR4 (FLAG-CXCR4) or FLAG-ACKR3 with human influenza haemagglutinin (HA)-tagged AVPR1A (HA-AVPR1A) in HEK293T cells and performed proximity ligation assays (PLAs) with anti-HA and anti-FLAG to visualize and quantify individual receptors and receptor–receptor interactions at single-molecule resolution [35]. Figure 2a shows representative PLA images for the detection of HA- and FLAG-tagged receptors and receptor–receptor interactions, and figure 2b shows the quantification of the corresponding PLA signals from three independent experiments. We observed positive

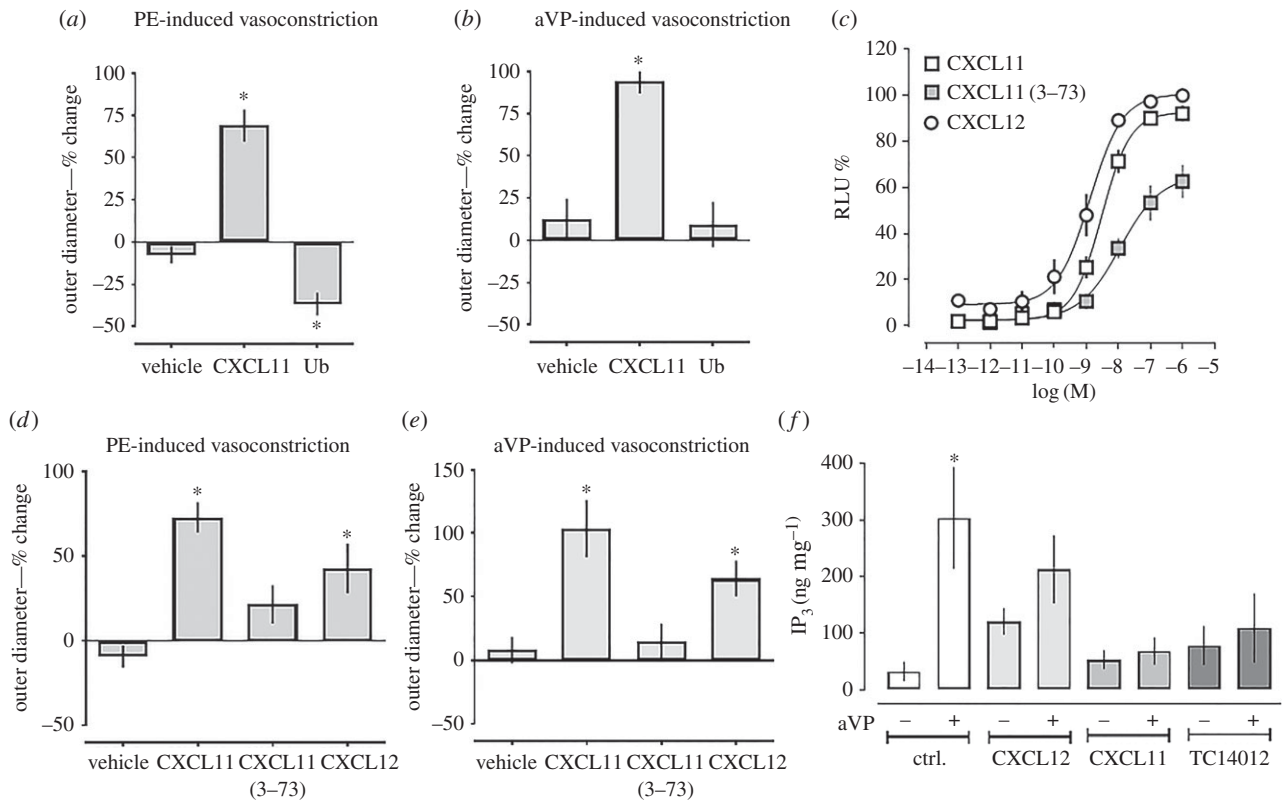


Figure 1. ACKR3 agonists antagonize aVP-mediated $G\alpha_q$ signalling and function in vascular smooth muscle. (a,b) Pressure myography with rat mesenteric arteries. Arteries were pressurized to 80 mmHg, precontracted with 2 μM PE (a) or 0.5 nM aVP (b), followed by the addition of vehicle ($n = 4$) or 10 μM of CXCL11 ($n = 6$) or ubiquitin ($n = 7$). Outer diameter % change: % change in outer diameter after the addition of the CXCR4/ACKR3 ligands. $*p < 0.05$ versus vehicle. (c) β -arrestin 2 recruitment assay (PRESTO-Tango) for ACKR3. HTLA cells were treated with CXCL12, CXCL11 or CXCL11 (3–73). RLU (%): relative luminescence units in % RLU after treatment with 1 μM CXCL12 (= 100%). $n = 3$ independent experiments. (d) Pressure myography experiments as in (a); PE-induced vasoconstriction. All ACKR3 ligands were tested at a concentration of 10 μM . Vehicle ($n = 5$), CXCL11 ($n = 7$), CXCL11 (3–73) ($n = 9$) and CXCL12 ($n = 14$). $*p < 0.05$ versus vehicle. (e) Pressure myography experiments as in (b); aVP-induced vasoconstriction. All ACKR3 ligands were tested at a concentration of 10 μM . Vehicle ($n = 4$), CXCL11 ($n = 3$), CXCL11 (3–73) ($n = 3$) and CXCL12 ($n = 3$). $*p < 0.05$ versus vehicle. (f) hVSMCs were pretreated with either vehicle (ctrl.) or ACKR3 ligands (1 μM , 15 min) and then stimulated with 1 μM aVP for 5 min. IP_3 production was measured by ELISA. $n = 4$. $*p < 0.05$ versus vehicle-treated cells.

signals corresponding to HA-AVPR1A:FLAG-ACKR3 interactions. By contrast, the number of PLA signals for HA-AVPR1A:FLAG-CXCR4 interactions was not significantly different from that of PLA signals in negative control experiments. To confirm the observation that HA-AVPR1A interacts with FLAG-ACKR3 in PLA experiments, we immunoprecipitated HA-AVPR1A with an anti-HA antibody and then performed western blot experiments with anti-HA and anti-FLAG to detect HA-AVPR1A and FLAG-ACKR3, respectively. As shown in figure 2c (left), when the cell lysate (input) was probed with anti-HA, we observed a band below 50 kDa and numerous bands in the high-molecular-mass range, which probably corresponds to the HA-AVPR1A monomer with the majority of receptors migrating as aggregates. The latter were also detectable in the HA-immunoprecipitate, but not in the IgG-immunoprecipitate. When probed with anti-FLAG (figure 2c, right), a similar pattern was detectable in the cell lysate, and both a faint band below 50 kDa and high-molecular aggregates were detectable in the HA-immunoprecipitate but not in the IgG-immunoprecipitate, indicating that FLAG-immunoreactivity could be precipitated with anti-HA.

Next, we used plasmids encoding AVPR1A-hRluc (*Renilla reniformis*), enhanced yellow fluorescent protein (EYFP) and ACKR3-EYFP for intermolecular BRET experiments (figure 2d,e). In cells expressing EYFP and AVPR1A-hRluc, the BRET signal was low and increased linearly with increasing

acceptor:donor ratios, which is consistent with a non-specific bystander BRET signal (figure 2d). The BRET signals in cells expressing ACKR3-EYFP and AVPR1A-hRluc showed a hyperbolic progression with increasing acceptor:donor ratios (figure 2d), and the BRET signal was independent of the concentrations of BRET partners when tested at a fixed acceptor:donor ratio (figure 2e), indicating constitutive heteromerization [36].

As PLA, co-immunoprecipitation and BRET assays collectively suggested that recombinant AVPR1A heteromerizes with ACKR3 when co-expressed, we tested whether such interactions are also detectable for endogenously expressed receptors using PLA to detect receptor-receptor interactions in hVSMC. The anti-GPCR antibodies that were used in PLA are directed against extracellular domains of the receptors and have been validated for sufficient selectivity for their GPCR targets previously [19,21,37]. Figure 3a shows representative PLA images and figure 3b shows the quantification of PLA signals for individual receptors and receptor interactions from four independent experiments. In line with our findings on recombinant receptors, we observed positive PLA signals for endogenous ACKR3:AVPR1A interactions, whereas signals for CXCR4:AVPR1A interactions were indistinguishable from negative control experiments. Furthermore, we observed that PLA signals for phosphorylated (Ser-19) myosin light chain (pMLC) 2 (figure 3a, bottom left) were indistinguishable from negative controls in cells that were not permeabilized,

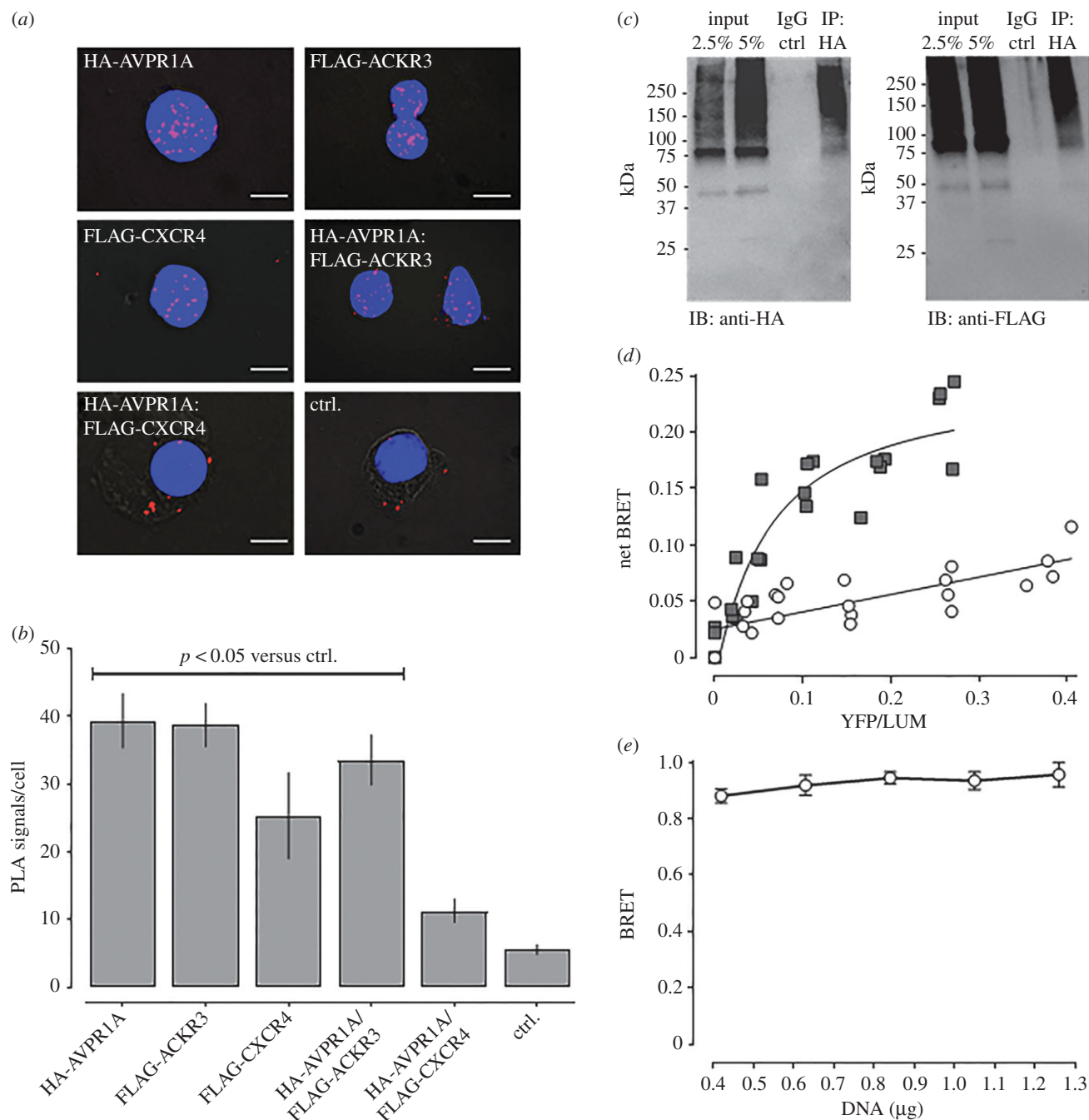


Figure 2. Recombinant ACKR3 and AVPR1A form heteromeric complexes. (a) Typical PLA images for the detection of individual receptors and receptor-receptor interactions in HEK293T cells transfected with DNA encoding HA- or FLAG-tagged receptors. Ctrl: cells transfected with pcDNA. Images show merged PLA/DAPI signals acquired from z-stack images ($n = 10$; thickness $1 \mu\text{m}$, bottom to top). Scale bars, $10 \mu\text{m}$. (b) Quantification of PLA signals per cell as in (a). $n = 3$ independent experiments with $n = 10$ images per condition and experiment. (c) HEK293T cells expressing HA-AVPR1A and FLAG-ACKR3 were lysed (input), the lysate was immunoprecipitated (IP) with anti-HA, followed by immunoblotting (IB) to detect HA-AVPR1A (left) and FLAG-ACKR3 (right) in the IP samples. IP control: precipitate after incubation of cell lysates with IgG-coupled resin. (d,e) Intermolecular BRET assays. Cells were co-transfected with AVPR1A-hRluc plus EYFP (open circles) or ACKR3-EYFP (grey squares) at various acceptor:donor ratios (d) and with increasing amounts of AVPR1A-hRluc and ACKR3-EYFP at a constant ratio of 1:10 (e).

whereas positive PLA signals were detectable in cells after permeabilization (figure 3a, bottom right). In line with our previous findings [19], this observation is consistent with the intracellular localization of pMLC2 and demonstrates that antibodies do not reach intracellular compartments when PLA is performed in non-permeabilized cells. This indicates that the PLA signals for individual receptors and receptor interactions that were obtained with anti-GPCR antibodies directed against extracellular receptor domains in non-permeabilized hVSMCs are localized on the cell surface under our experimental

conditions. This assumption is supported by three-dimensional reconstruction of the PLA signals from deconvolved z-stack images, which showed that most PLA signals for ACKR3:AVPR1A interactions are localized in a single plane (figure 3c).

To confirm these observations, we performed immunoprecipitation experiments with hVSMC. AVPR1A could be precipitated with anti-AVPR1A (figure 3d). ACKR3 and CXCR4 were detectable in the AVPR1A immunoprecipitate (figure 3e,f). β_2 -AR, which was used as a negative control,

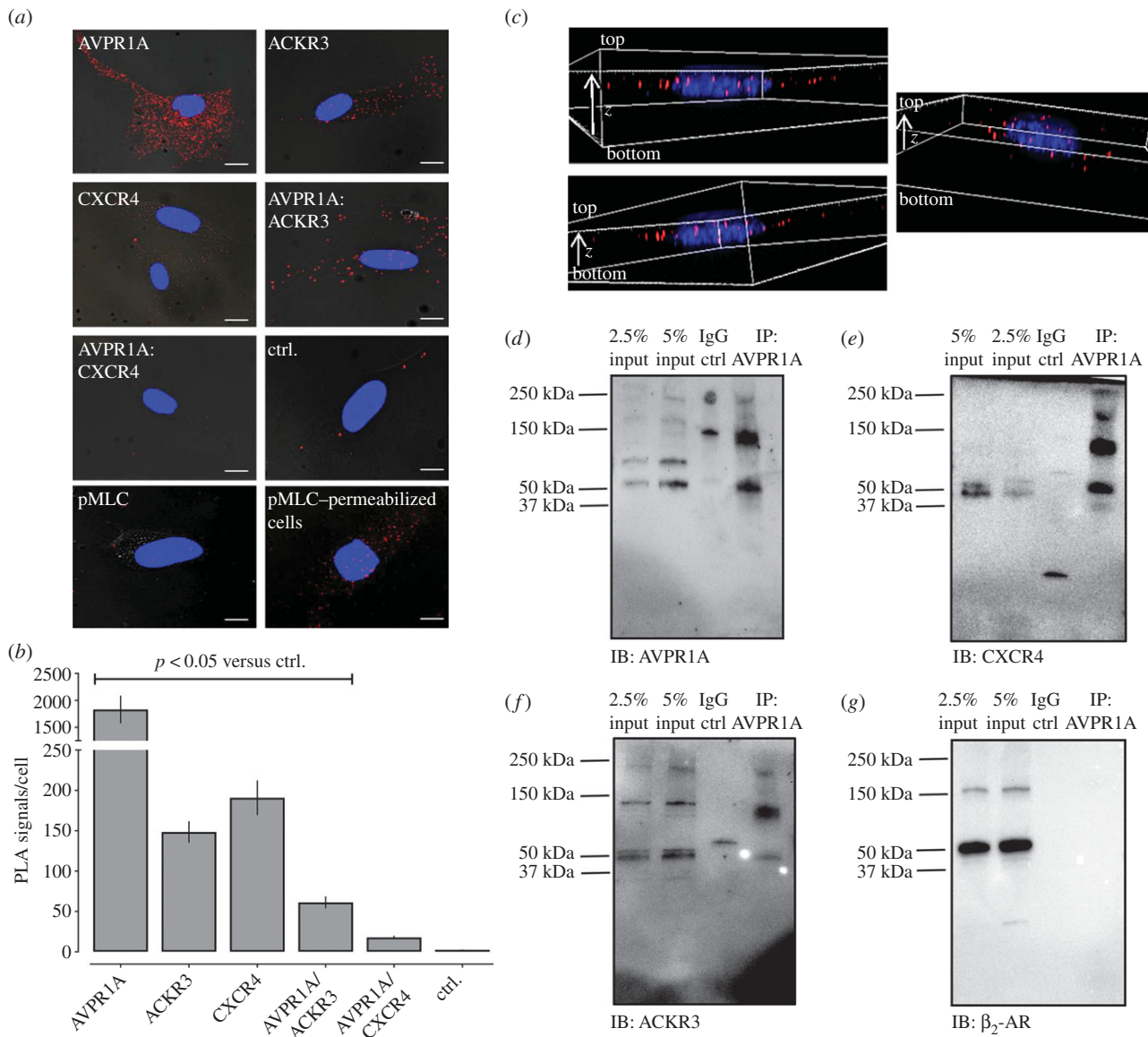


Figure 3. ACKR3 and AVPR1A form heteromeric complexes in hVSMCs. (a) Representative PLA images for the detection of individual receptors, receptor–receptor complexes and pMLC in hVSMC. PLA for pMLC2 was performed in non-permeabilized cells (pMLC2, bottom left) and permeabilized cells (pMLC2, permeabilized cells, bottom right). All other PLAs were performed in non-permeabilized cells. Ctrl: omission of one primary antibody. Images show merged PLA/DAPI signals acquired from z-stack images ($n = 10$; thickness $1 \mu\text{m}$, bottom to top). Scale bars, $10 \mu\text{m}$. (b) Quantification of PLA signals per cell as in (a). $n = 4$ independent experiments with $n = 10$ images per condition and experiment. (c) Three-dimensional representations of ACKR3 : AVPR1A interactions in hVSMC. Deconvolved images were generated from z-stack images ($n = 20$; thickness: $0.5 \mu\text{m}$, bottom to top). Images show merged PLA/DAPI signals. (d–g) hVSMCs were lysed (=input) and AVPR1A was immunoprecipitated (IP) followed by immunoblotting (IB) to detect AVPR1A (d), CXCR4 (e), ACKR3 (f) and β_2 -AR (g) in the IP samples. IP control: precipitate after incubation of cell lysates with IgG-coupled resin. Images are representative of $n = 4$ independent experiments.

could not be detected (figure 3g). The combination of the findings that positive PLA, co-immunoprecipitation and BRET signals were detectable for recombinant ACKR3 : AVPR1A interactions, that positive PLA signals for endogenous ACKR3 : AVPR1A interactions were detectable and that endogenous ACKR3 could be co-immunoprecipitated with AVPR1A indicates that both receptors form heteromeric complexes in hVSMC. As CXCR4 is known to form heteromeric complexes with ACKR3 [10,11,19], the findings that CXCR4 was detectable in AVPR1A immunoprecipitates, despite the lack of significant PLA signals for CXCR4 : AVPR1A interactions, could suggest that CXCR4 exists within the same plasma membrane microdomains as ACKR3 and AVPR1A, but is not in sufficient proximity to AVPR1A to permit direct interactions. Alternatively, it appears possible that the abundance of CXCR4 : AVPR1A interactions

is too low to be discriminated with confidence by PLA under our experimental conditions.

2.3. Depletion of ACKR3 : AVPR1A heteromers by ACKR3 knockdown increases AVPR1A : CXCR4 heteromerization and inhibits aVP-induced $G\alpha_q$ signalling

To evaluate functional consequences of ACKR3 : AVPR1A heteromerization on AVPR1A signalling in hVSMC, we depleted ACKR3 : AVPR1A heteromers by ACKR3 knockdown with siRNA. Figure 4 shows typical PLA images for the detection of individual receptors (figure 4a), receptor–receptor

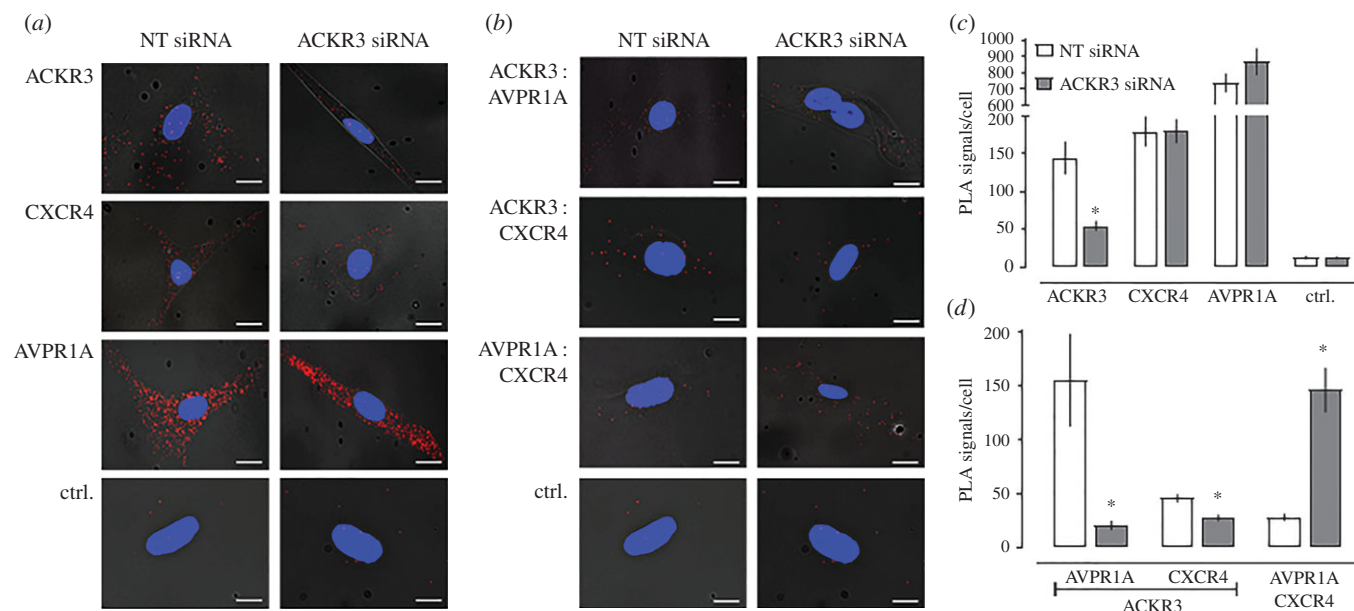


Figure 4. ACKR3 gene silencing reduces ACKR3 : AVPR1A and ACKR3 : CXCR4 heteromers and increases AVPR1A : CXCR4 interactions in hVSMCs. (a,b) Representative PLA images for the detection of individual receptors (a) and receptor–receptor interactions (b) in hVSMC after incubation with NT or ACKR3 siRNA. Ctrl: omission of one primary antibody. Images show merged PLA/4',6-diamidino-2-phenylindole dihydrochloride (DAPI) signals acquired from z-stack images ($n = 10$; thickness $1 \mu\text{m}$, bottom to top). (c,d) Quantification of PLA signals per cell for the detection of individual receptors (c) and receptor–receptor interactions (d) as in (a,b). $n = 4$ independent experiments with $n = 10$ images per condition and experiment. * $p < 0.05$ versus cells incubated with NT-siRNA.

interactions (figure 4b) and the quantification of the number of corresponding PLA signals from four independent experiments (figure 4c,d). When compared with hVSMC after incubation with non-targeting (NT) siRNA, PLA signals for ACKR3 were reduced by more than 60% after incubation with ACKR3 siRNA (figure 4c). PLA signals for CXCR4 and AVPR1A were indistinguishable in hVSMC incubated with NT and ACKR3 siRNA (figure 4c). When PLA was performed to detect receptor–receptor interactions (figure 4d), we observed that signals corresponding to ACKR3 : AVPR1A and ACKR3 : CXCR4 heteromers in hVSMC incubated with ACKR3 siRNA were reduced by 80% and 50%, respectively, when compared with hVSMC incubated with NT-siRNA. Surprisingly, in hVSMC incubated with ACKR3 siRNA, PLA signals corresponding to CXCR4 : AVPR1A interactions increased to 510% of PLA signals in hVSMC incubated with NT-siRNA. To confirm these observations, we repeated the siRNA knockdown experiments in the rat vascular smooth muscle cell line A7r5. Figure 5 shows typical PLA images for the detection of individual receptors (figure 5a), receptor–receptor interactions (figure 5b) and the quantification of the number of corresponding PLA signals from six independent experiments (figure 5c,d). As in hVSMC, we also observed positive PLA signals for ACKR3 : AVPR1A heteromers in A7r5 cells. While rat and human ACKR3 show 93% sequence identity, rat and human AVPR1A share only 79% sequence identity [38]. The positive PLA signals for ACKR3 : AVPR1A heteromers in A7r5 cells indicate that these differences between the rat and human AVPR1A sequences do not affect interactions between the receptor partners. Similar to hVSMC, we observed that ACKR3 depletion in A7r5 cells by siRNA knockdown reduced PLA signals for ACKR3 : AVPR1A and ACKR3 : CXCR4 interactions proportional to the degree of ACKR3 knockdown, but increased PLA signals for CXCR4 : AVPR1A interactions to 276% of PLA signals in A7r5 cells incubated with NT-siRNA. These findings suggest that ACKR3 hinders CXCR4 : AVPR1A interactions, which occur after depletion of

ACKR3 from the cell surface. Such a behaviour would be in agreement with previous observations, indicating that hetero-oligomeric receptor complexes within the plasma membrane exist in a dynamic equilibrium, in which interference with heteromerization between two receptors shifts the patterns of receptor hetero-oligomerization within the entire receptor network towards a new equilibrium, leading to newly formed heteromeric receptor complexes [21,39–41]. Furthermore, these observations imply that the insignificant number of PLA signals for CXCR4 : AVPR1A interactions that were detectable in hVSMC probably corresponds to a very low abundance of CXCR4 : AVPR1A heteromers.

To assess the effect of CXCR4 knockdown on the formation of heteromeric complexes between AVPR1A and ACKR3 or CXCR4 in hVSMC, we then silenced CXCR4 with siRNA. Figure 6a shows representative PLA images for the detection of CXCR4 and of CXCR4 : AVPR1A and ACKR3 : AVPR1A heteromers in hVSMC incubated with NT or CXCR4 siRNA, and figure 6b shows the quantification of corresponding PLA signals from four independent experiments. When compared with hVSMC incubated with NT-siRNA, PLA signals for CXCR4 were reduced by 70% after incubation with CXCR4 siRNA. While PLA signals for CXCR4 : AVPR1A interactions decreased to the same degree, CXCR4 silencing did not affect the number of PLA signals for ACKR3 : AVPR1A interactions.

These findings suggest that AVPR1A preferentially forms heteromeric complexes with ACKR3 and CXCR4 protomers or homodimers, but not with CXCR4 : ACKR3 heteromers. This interaction pattern is similar to the interaction pattern that we previously observed for α_{1A} -AR : CXCR4 and α_{1A} -AR : ACKR3 heteromers, and distinct from the interaction pattern of $\alpha_{1B/D}$ -AR, which preferentially form hetero-oligomeric complexes with the CXCR4 : ACKR3 heteromer [21].

Measurements of aVP-induced IP₃ production in hVSMC after ACKR3 and CXCR4 silencing with siRNA are shown in figure 6c. While there were no significant differences in aVP-induced IP₃ production in hVSMC incubated with NT and

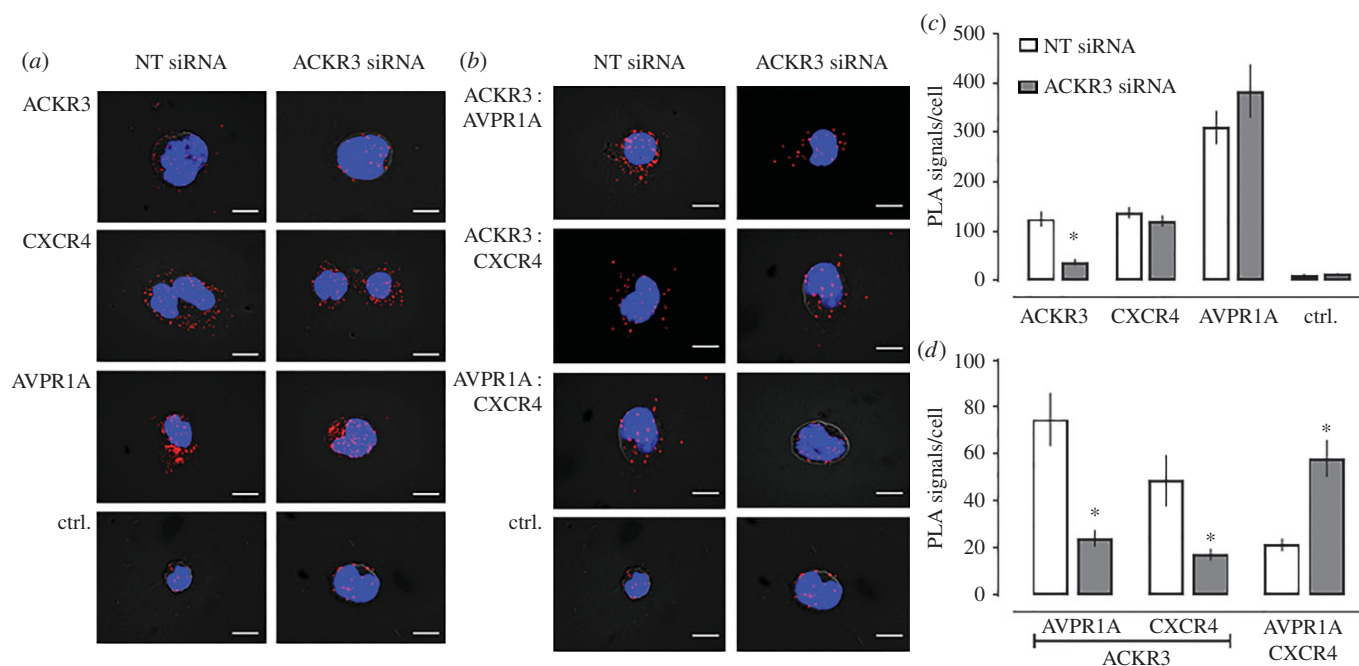


Figure 5. ACKR3 gene silencing reduces ACKR3 : AVPR1A and ACKR3 : CXCR4 heteromers and increases AVPR1A : CXCR4 interactions in A7r5 cells. (a,b). Representative PLA images for the detection of individual receptors (a) and receptor–receptor interactions (b) in A7r5 cells after incubation with NT or ACKR3 siRNA. Ctrl: omission of one primary antibody. Images show merged PLA/4',6-diamidino-2-phenylindole dihydrochloride (DAPI) signals acquired from z-stack images ($n = 10$; thickness $1 \mu\text{m}$, bottom to top). (c,d) Quantification of PLA signals per cell for the detection of individual receptors (c) and receptor–receptor interactions (d) as in (a,b). $n = 6$ independent experiments with $n = 10$ images per condition and experiment. * $p < 0.05$ versus cells incubated with NT-siRNA.

CXCR4 siRNA, aVP-induced IP_3 production in hVSMC was abolished after incubation with ACKR3 siRNA. These findings indicate that heteromerization between AVPR1A and ACKR3 is required for AVPR1A signalling in hVSMC, which is similar to the requirement of hetero-oligomerization between $\alpha_{1B/D}$ -AR and the CXCR4 : ACKR3 heteromeric complex for $\alpha_{1B/D}$ -AR signalling in hVSMC that we described previously [21]. While ACKR3 within the ACKR3 : AVPR1A complex may serve to stabilize AVPR1A in a configuration capable of coupling to G_{α_q} , it appears also possible that the formation of AVPR1A : CXCR4 heteromers after ACKR3 silencing could be responsible for the loss of aVP-induced IP_3 production. The latter would imply that CXCR4 within the heteromeric AVPR1A : CXCR4 complex hinders AVPR1A signalling upon agonist stimulation.

2.4. Transmembrane domain-derived peptide analogues of ACKR3 interfere with AVPR1A : ACKR3 heteromerization and aVP-induced G_{α_q} signalling

TM-derived peptide analogues of GPCRs have previously been used to disrupt heteromerization and alter receptor function [19–21,42–44]. Thus, we tested whether TM2, TM4 and TM7 peptide analogues of ACKR3 interfere with AVPR1A : ACKR3 heteromerization. Representative images from PLA for the detection of individual receptors and receptor–receptor interactions in hVSMC incubated with vehicle or TM peptides are shown in figure 7, and the quantifications of corresponding PLA signals from three independent experiments are shown in figure 8a,b. The TM peptides did not affect PLA signals for AVPR1A, ACKR3 or CXCR4 (figure 8a). Furthermore, none of the TM peptides affected PLA signals for AVPR1A : CXCR4 interactions (figure 8b). While the TM2 and TM4 peptides reduced PLA signals for AVPR1A : ACKR3 interactions, all TM peptide analogues reduced PLA signals for CXCR4 :

ACKR3 interactions. These findings confirm our previous observations on the effects of the TM peptides on CXCR4 : ACKR3 heteromerization and mimic their effects on the formation of heteromeric complexes between α_{1B} -AR and ACKR3 [21]. The latter suggests that α_{1B} -AR and AVPR1A may form heteromeric complexes via similar interaction sites on ACKR3.

The effects of the TM peptide analogues on aVP-induced IP_3 production in hVSMC are shown in figure 8c. Consistent with their effects on ACKR3 : AVPR1A heteromerization, we observed that the TM2 and TM4 peptide analogues inhibited aVP-induced IP_3 production in hVSMC, whereas the TM7 peptide analogue was ineffective. To address the possibility that the TM peptides directly affect AVPR1A function, we performed β -arrestin 2 recruitment assays for AVPR1A. As shown in figure 8d, none of the peptides affected β -arrestin 2 recruitment to AVPR1A upon aVP stimulation. These findings are in agreement with the loss of aVP-responsiveness of hVSMC after ACKR3 silencing, and further suggest that heteromerization between AVPR1A and ACKR3 is required for AVPR1A signalling in hVSMC. Because the TM2 and TM4 peptide analogues did not increase AVPR1A : CXCR4 interactions, formation of such interactions cannot account for the loss of aVP-responsiveness. This supports the concept that ACKR3 within the ACKR3 : AVPR1A complex serves to stabilize AVPR1A in a functional configuration.

2.5. The AVPR1A : ACKR3 heteromeric complex modulates β -arrestin recruitment to each receptor partner and shows asymmetrical β -arrestin cross-recruitment upon agonist stimulation

We used the PRESTO-Tango cell system to evaluate whether heteromerization between AVPR1A and ACKR3 also

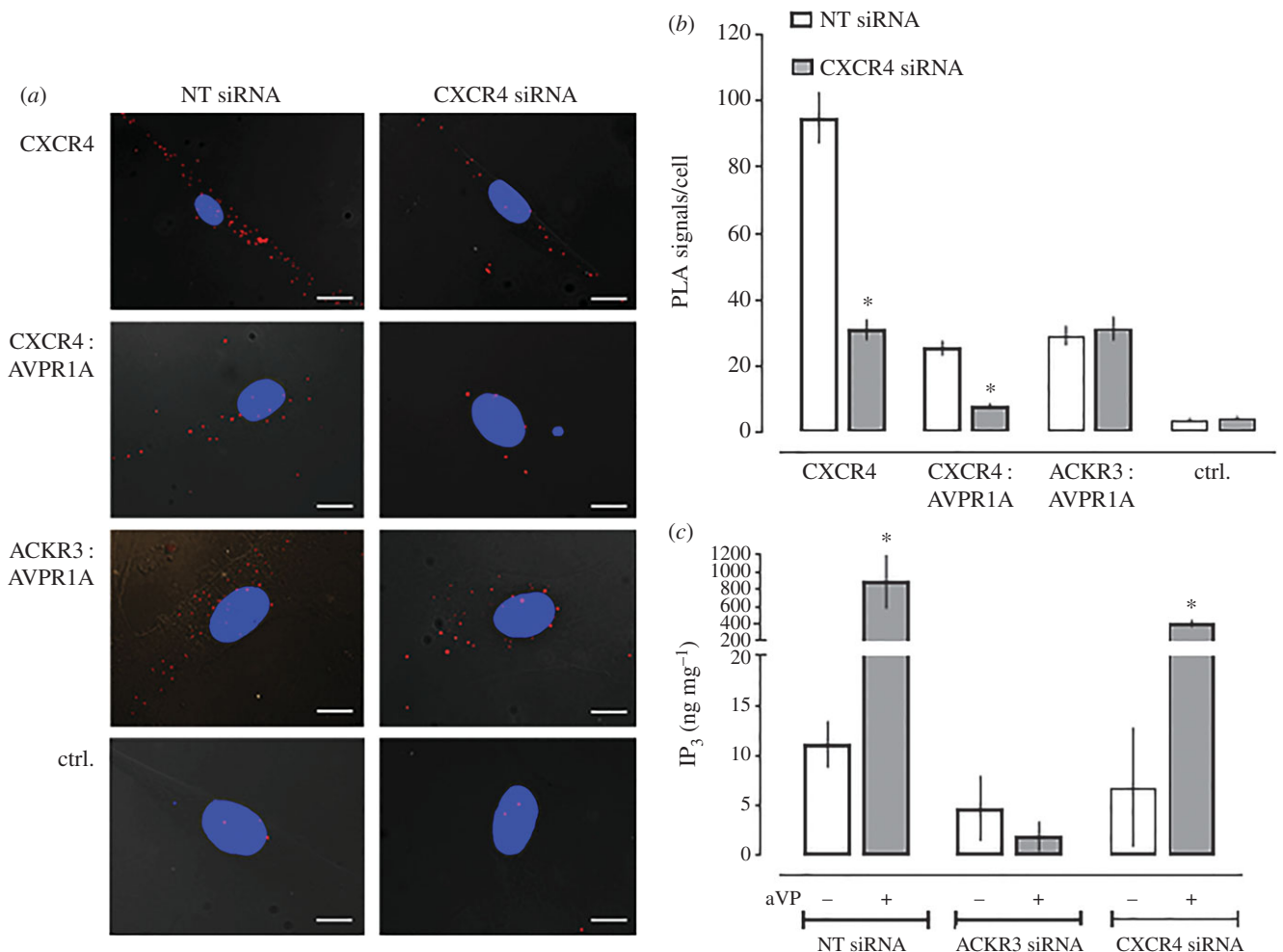


Figure 6. ACKR3 gene silencing inhibits aVP-mediated $G\alpha_q$ signalling, whereas CXCR4 gene silencing does not affect ACKR3 : AVPR1A heteromerization and aVP-mediated $G\alpha_q$ signalling. (a) Representative PLA images for the detection of CXCR4 and receptor–receptor interactions in hVSMC after incubation with NT or CXCR4 siRNA. Ctrl: omission of one primary antibody. Images show merged PLA/4',6-diamidino-2-phenylindole dihydrochloride (DAPI) signals acquired from z-stack images ($n = 10$; thickness 1 μm , bottom to top). Scale bars, 10 μm . (b) Quantification of PLA signals per cell as in (a). $n = 4$ independent experiments with $n = 10$ images per condition and experiment. * $p < 0.05$ versus cells incubated with NT-siRNA. (c) IP₃ production of hVSMC incubated with NT, ACKR3 or CXCR4 siRNA upon stimulation with vehicle (–) or 1 μM aVP (+) for 5 min. $n = 4$ independent experiments. * $p < 0.05$ versus vehicle.

modulates β -arrestin 2 recruitment upon agonist stimulation. We first co-expressed FLAG-AVPR1A-Tango with pcDNA3 or HA-ACKR3, confirmed comparable FLAG-AVPR1A-Tango expression by flow cytometry (figure 9a) and determined the dose–response for β -arrestin 2 recruitment upon agonist stimulation (figure 9b). In cells co-expressing AVPR1A-Tango/pcDNA3, aVP induced β -arrestin 2 recruitment with an EC_{50} (95% CI) of 2.5 (0.8–8.8) nM and top plateau was 97 ± 7 RLU%. While the potency of aVP to recruit β -arrestin 2 in cells co-expressing AVPR1A-Tango/ACKR3 was similar to cells co-expressing AVPR1A-Tango/pcDNA3 (EC_{50} (95% CI): 6.1 (0.7–58) nM, $p > 0.05$ versus AVPR1A-Tango/pcDNA3), the efficacy of aVP was significantly reduced (top plateau: 32 ± 4 RFU%, $p < 0.001$ versus AVPR1A-Tango/pcDNA3). CXCL11 and CXCL12 did not induce β -arrestin 2 recruitment to AVPR1A-Tango in the presence or absence of ACKR3 (figure 9c). When cells co-expressing similar levels of ACKR3-Tango plus pcDNA3 or AVPR1A (figure 9d) were tested, we observed that the presence of AVPR1A significantly reduced the efficacy of CXCL11 (figure 9e) and CXCL12 (figure 9f) to recruit β -arrestin 2 to ACKR3-Tango, without affecting the potency of the ACKR3 agonists. While aVP stimulation did not induce β -arrestin 2 recruitment to ACKR3-Tango when co-expressed with pcDNA3, aVP induced β -arrestin 2

recruitment to ACKR3-Tango when co-expressed with AVPR1A (figure 9g).

The effects of the TM peptide analogues of ACKR3 on aVP-induced recruitment of β -arrestin 2 to ACKR3-Tango in cells co-expressing ACKR3-Tango and AVPR1A are shown in figure 9h. When compared with vehicle-treated cells, the TM2 and TM4 peptide analogues significantly reduced the efficacy of aVP to induce β -arrestin 2 recruitment, whereas the TM7 peptide did not show significant effects. Recently, we reported that the TM2 peptide analogue shows the pharmacological behaviour of a competitive antagonist for β -arrestin 2 recruitment to ACKR3-Tango upon agonist stimulation, whereas the TM7 peptide analogue was inactive; the TM4 peptide exhibited a behaviour similar to the TM2 peptide, but this effect did not reach statistical significance [21]. In the present study, the TM2 and TM4 peptides showed the pharmacological behaviour of non-competitive antagonists, which inhibited aVP-induced β -arrestin 2 recruitment to ACKR3-Tango with comparable efficacy. This behaviour is consistent with the notion that interference of the TM2/4 peptides with ACKR3 : AVPR1A heteromerization is the main mechanism underlying their inhibitory effects on aVP-induced β -arrestin 2 recruitment to ACKR3-Tango in cells co-expressing ACKR3-Tango and AVPR1A.

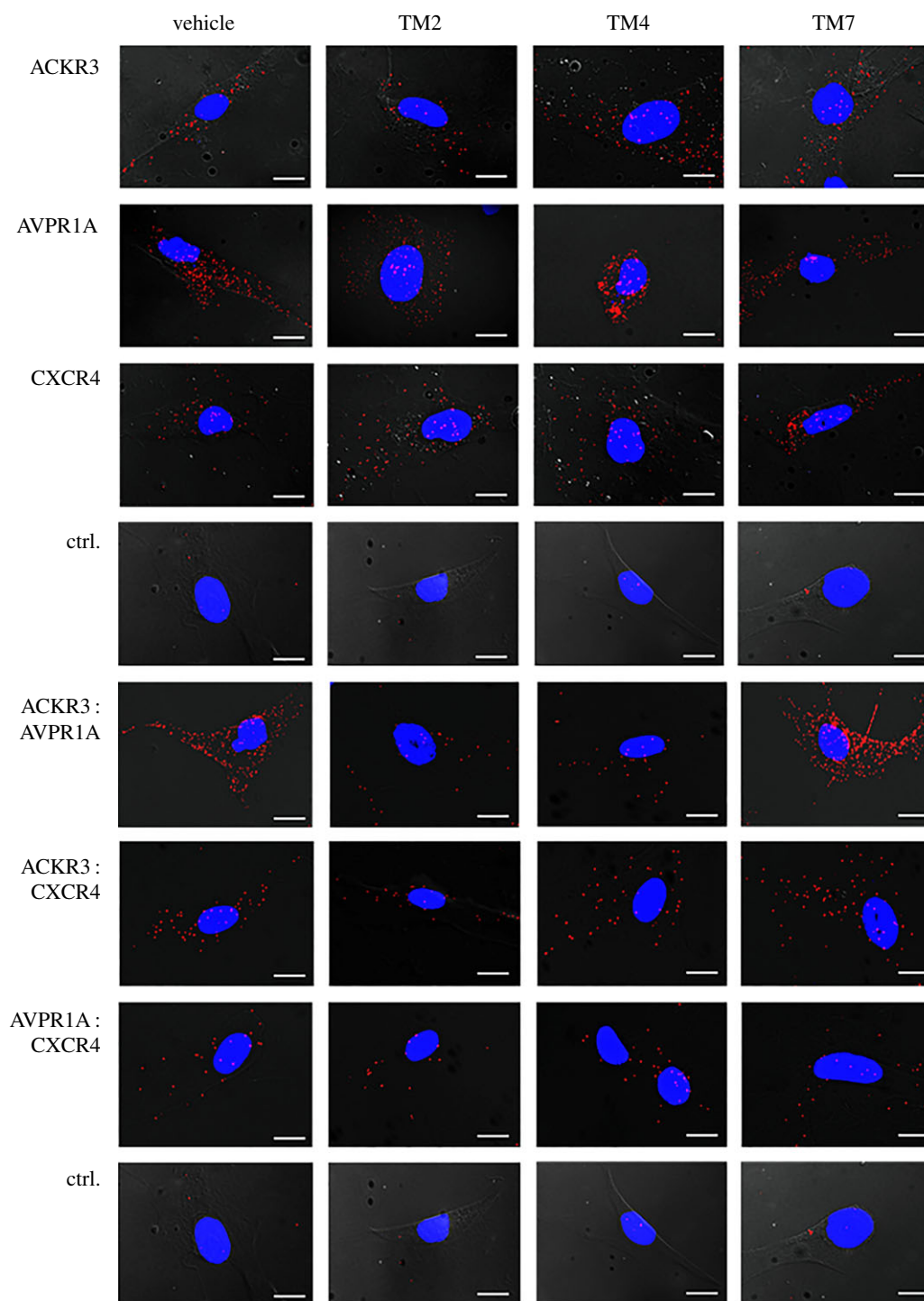


Figure 7. ACKR3-derived TM peptide analogues disrupt ACKR3 : AVPR1A and ACKR3 : CXCR4 heteromeric complexes. hVSMCs were incubated with vehicle, TM2, TM4 or TM7 (10 μ M, 30 min at 37°C), washed and fixed for PLA. Typical PLA images for the detection of individual receptors or receptor–receptor complexes are shown. Ctrl: omission of one primary antibody. Images show merged PLA/4',6-diamidino-2-phenylindole dihydrochloride (DAPI) signals acquired from z-stack images ($n = 10$; thickness 1 μ m, bottom to top). Scale bars, 10 μ m.

Our observation that the presence of ACKR3 reduces aVP-induced β -arrestin 2 recruitment to AVPR1A-Tango and that the presence of AVPR1A enables β -arrestin 2 recruitment to ACKR3-Tango upon aVP stimulation indicates that AVPR1A activation within the heteromeric AVPR1A : ACKR3 complex leads to β -arrestin 2 recruitment to both receptor partners. CXCL11 and CXCL12, however, failed to cross-recruit β -arrestin 2 to AVPR1A-Tango in the presence of ACKR3. These findings imply that ACKR3 within the heteromeric receptor complex attenuates β -arrestin 2 recruitment to AVPR1A via allosteric interactions. In combination with the observed effects of AVPR1A : ACKR3

heteromerization on aVP-induced $G\alpha_q$ -mediated signalling events, these data suggest that ACKR3 within the AVPR1A : ACKR3 heteromer controls the balance between AVPR1A-mediated $G\alpha_q$ and β -arrestin signalling. Furthermore, our findings demonstrate asymmetrical agonist-induced cross-regulation of ACKR3 by AVPR1A within the heteromeric receptor complex. Such pharmacological behaviour of the AVPR1A : ACKR3 heteromeric complex is similar to the signalling behaviour of other GPCR heteromers, for which ligand-induced symmetrical and asymmetrical cross-activation and cross-inhibition of various signalling read-outs have previously been described [45–48].

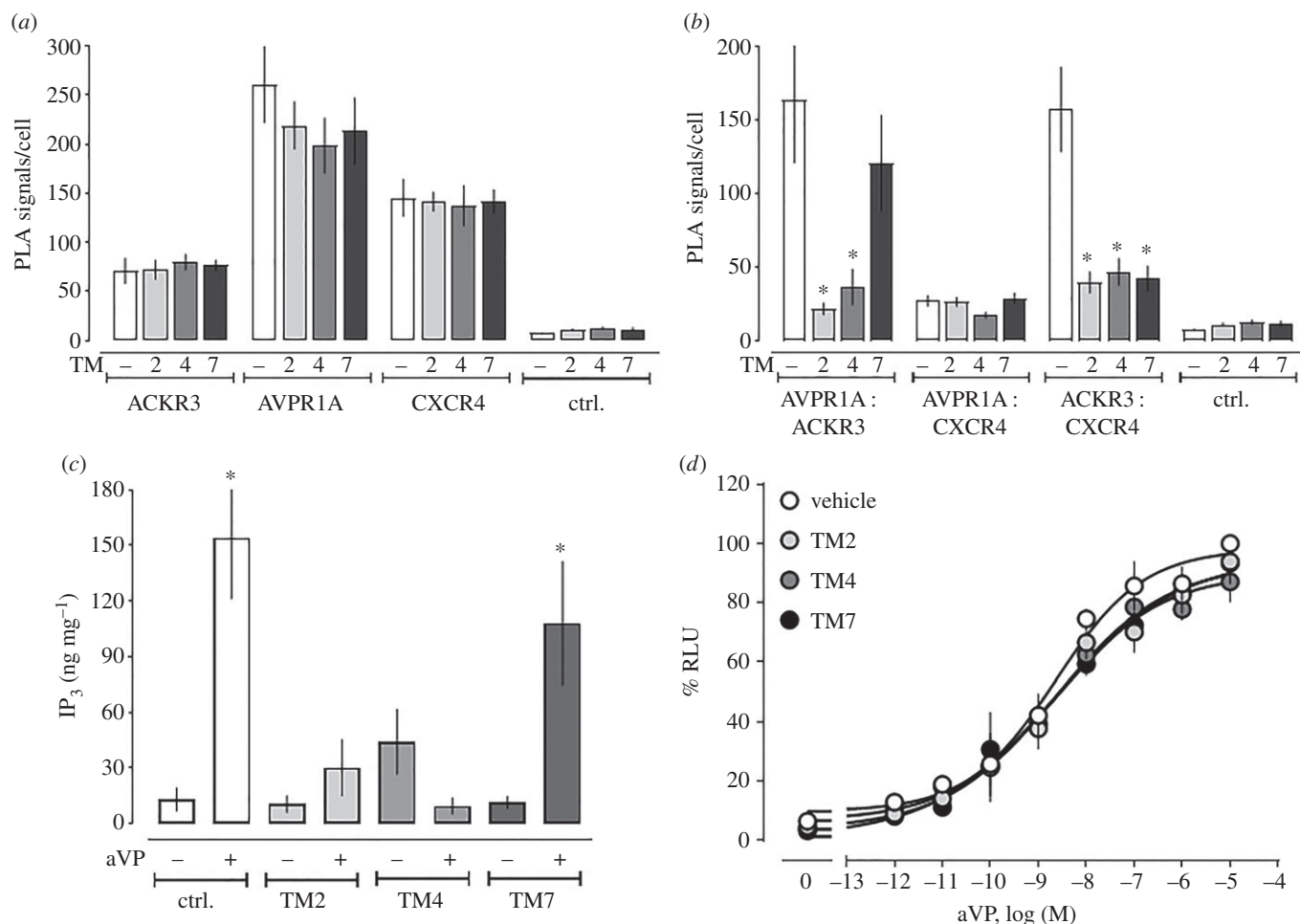


Figure 8. ACKR3-derived TM peptide analogues interfere with ACKR3:AVPR1A and ACKR3:CXCR4 heteromerization and inhibit aVP-induced $G\alpha_q$ signalling in hVSMC. (a,b) Quantification of PLA signals per cell as in figure 7 for individual receptors (a) and receptor–receptor interactions (b). $n = 4$ independent experiments with $n = 10$ images per condition and experiment. $*p < 0.05$ versus cells incubated with vehicle. (c) IP_3 production was measured in hVSMC pretreated with vehicle or TM2/4/7 peptide analogues ($10 \mu\text{M}$, 30 min at 37°C) and then stimulated with either vehicle (–) or aVP ($1 \mu\text{M}$, 5 min) (+). $n = 4$ independent experiments. $*p < 0.05$ versus vehicle-treated cells. (d) β -arrestin 2 recruitment assay (PRESTO-Tango) for AVPR1A. HTLA cells expressing FLAG-AVPR1A-Tango were incubated with either vehicle or ACKR3 TM2/4/7 ($10 \mu\text{M}$, 30 min at 37°C) and then stimulated with aVP overnight. RLU (%): relative luminescence units in % RLU after treatment with $10 \mu\text{M}$ aVP (=100%). $n = 3$ independent experiments.

2.6. AVPR1A and ACKR3 co-internalize upon agonist binding

Agonist-induced β -arrestin recruitment to AVPR1A and ACKR3 is known to lead to the reduction of receptor cell surface expression levels, either via induction of receptor internalization or inhibition of receptor recycling [9,49,50]. As activation of recombinant AVPR1A cross-recruited β -arrestin 2 to ACKR3-Tango, we tested whether endogenous AVPR1A and ACKR3 in hVSMC co-internalize upon agonist stimulation. Thus, we stimulated hVSMC with aVP or CXCL11 and quantified AVPR1A and ACKR3 cell surface expression via double-immunofluorescence staining by flow cytometry. Figure 10a shows representative two-dimensional scatter plots for the detection of both receptors over a 60-minute time period after stimulation of hVSMC with aVP or CXCL11, and figure 10b,c shows the quantification of receptor cell surface expression from three independent experiments. aVP and CXCL11 stimulation of hVSMC time-dependently reduced expression levels of both AVPR1A and ACKR3. The time course and the degree of receptor depletion from the cell surface were comparable for both agonists, indicating symmetrical agonist-induced co-internalization of AVPR1A and

ACKR3. The finding that AVPR1A and ACKR3 co-internalize upon aVP stimulation matches well with the observed aVP-induced β -arrestin 2 cross-recruitment to ACKR3 within the AVPR1A:ACKR3 complex. CXCL11, however, failed to cross-recruit β -arrestin 2 to recombinant AVPR1A-Tango, yet induced co-internalization of both endogenous receptors. Thus, it appears possible that β -arrestin recruitment to only one of the two receptor partners within the heteromeric complex is sufficient to induce receptor co-internalization.

Taken together, our observations that endogenous AVPR1A and ACKR3 are in close proximity in hVSMC, that the association between endogenous AVPR1A and ACKR3 can be disrupted with selective ACKR3-derived TM peptide analogues without altering expression levels of the individual receptors, and that interference with the association between AVPR1A and ACKR3 in hVSMC alters receptor function fulfil recently proposed criteria for GPCR heteromers in native tissues [51]. While we currently cannot provide direct and unequivocal evidence for the localization of AVPR1A:ACKR3 heteromers on the plasma membrane, our finding that antibodies do not reach intracellular compartments in PLA when cells are not permeabilized, along with the observed changes in AVPR1A function upon exposure of cells to the

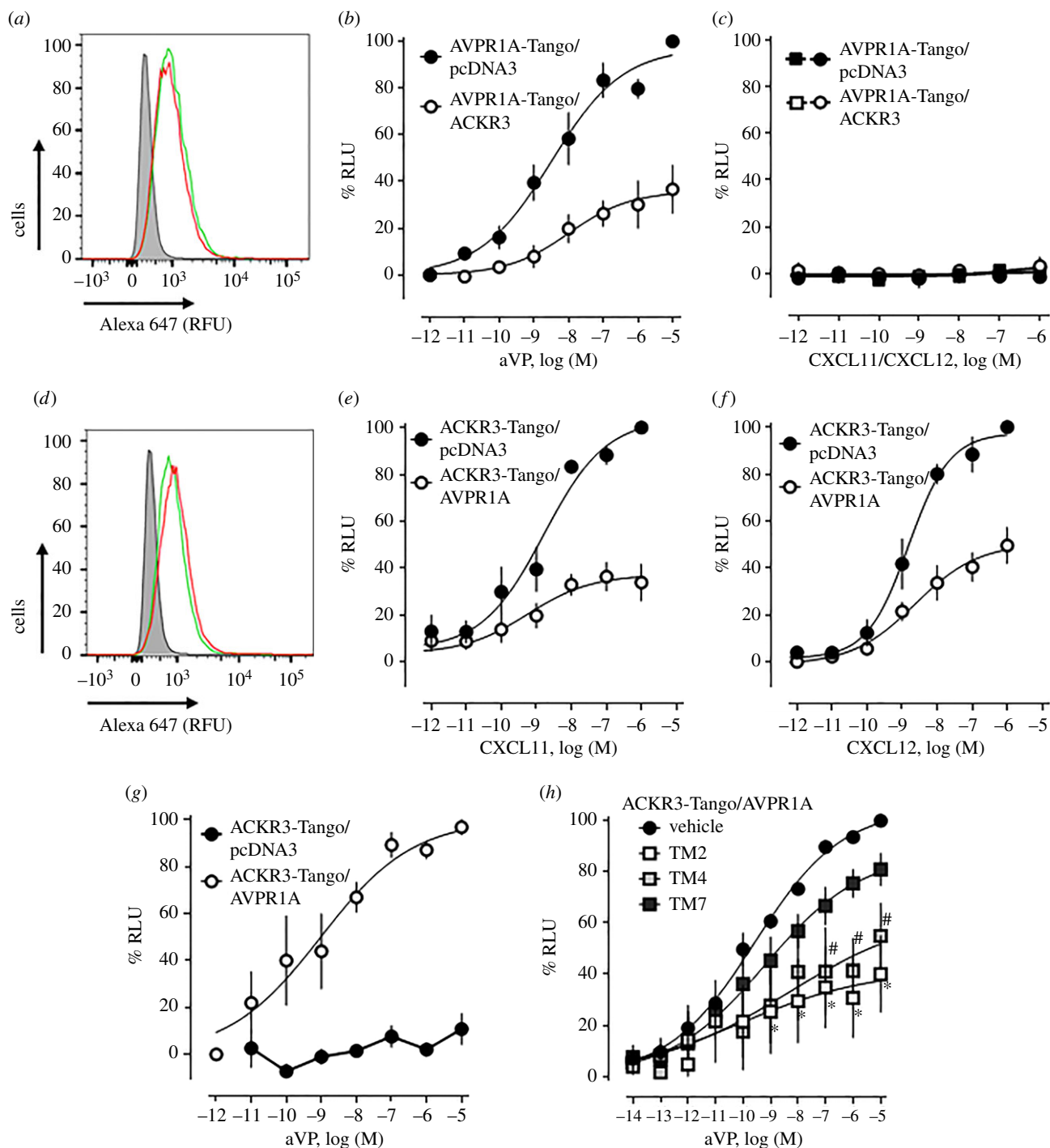


Figure 9. β -arrestin 2 recruitment at the ACKR3:AVPR1A heteromeric complex. (a–c) HTLA cells were co-transfected with 0.75 μ g of DNA for FLAG-AVPR1A-TANGO plus 0.75 μ g of pcDNA3 or HA-ACKR3. (a) Measurement of FLAG-AVPR1A-Tango expression by flow cytometry. Cells were labelled with Alexa Fluor 647 anti-FLAG. Grey area: unstained cells. Red line: cells transfected with FLAG-AVPR1A-TANGO plus pcDNA. Green line: cells transfected with FLAG-AVPR1A-TANGO/HA-ACKR3. RFU: relative fluorescence units. Data are representative of $n = 3$ independent experiments. (b,c) β -arrestin 2 recruitment assay (PRESTO-Tango) for AVPR1A. Cells were stimulated with aVP (b), CXCL11 (c) and CXCL12 (c). Black symbols: cells transfected with FLAG-AVPR1A-TANGO/pcDNA3; white symbols: cells transfected with FLAG-AVPR1A-TANGO/HA-ACKR3. $n = 3$ independent experiments. (d–g) HTLA cells were co-transfected with 0.75 μ g of DNA for FLAG-ACKR3-TANGO plus 0.75 μ g of pcDNA3 or HA-AVPR1A. (d) Measurement of FLAG-ACKR3-Tango expression by flow cytometry. Cells were labelled with Alexa Fluor 647 anti-FLAG. Grey area: unstained cells. Red line: cells transfected with FLAG-ACKR3-TANGO plus pcDNA3. Green line: cells transfected with FLAG-ACKR3-TANGO/HA-AVPR1A. RFU: relative fluorescence units. Data are representative of $n = 3$ experiments. (e–g) β -arrestin 2 recruitment assay (PRESTO-Tango) for ACKR3. Cells were stimulated with CXCL11 (e), CXCL12 (f) and aVP (g). Black circles: cells transfected with FLAG-ACKR3-TANGO/pcDNA3; white circles: cells transfected with FLAG-ACKR3-TANGO/HA-AVPR1A. $n = 3$ independent experiments. (h) β -arrestin 2 recruitment assay (PRESTO-Tango) with HTLA cells co-expressing FLAG-AVPR1A-Tango/HA-ACKR3. Cells were treated with vehicle or TM2/4/7 peptides (10 μ M, 30 min at 37°C) and then stimulated with aVP. $n = 3$ independent experiments. Black circle: vehicle. Open squares: TM2. Light grey squares: TM4. Dark grey squares: TM7. $n = 4$ independent experiments.

extracellular agonist after disruption of the AVPR1A:ACKR3 complexes, strongly suggests that these receptor heteromers are located on the plasma membrane. This notion is supported by

our findings in expression systems, which provide additional mechanistic insights into molecular events at the AVPR1A:ACKR3 heteromer and demonstrate that heteromerization

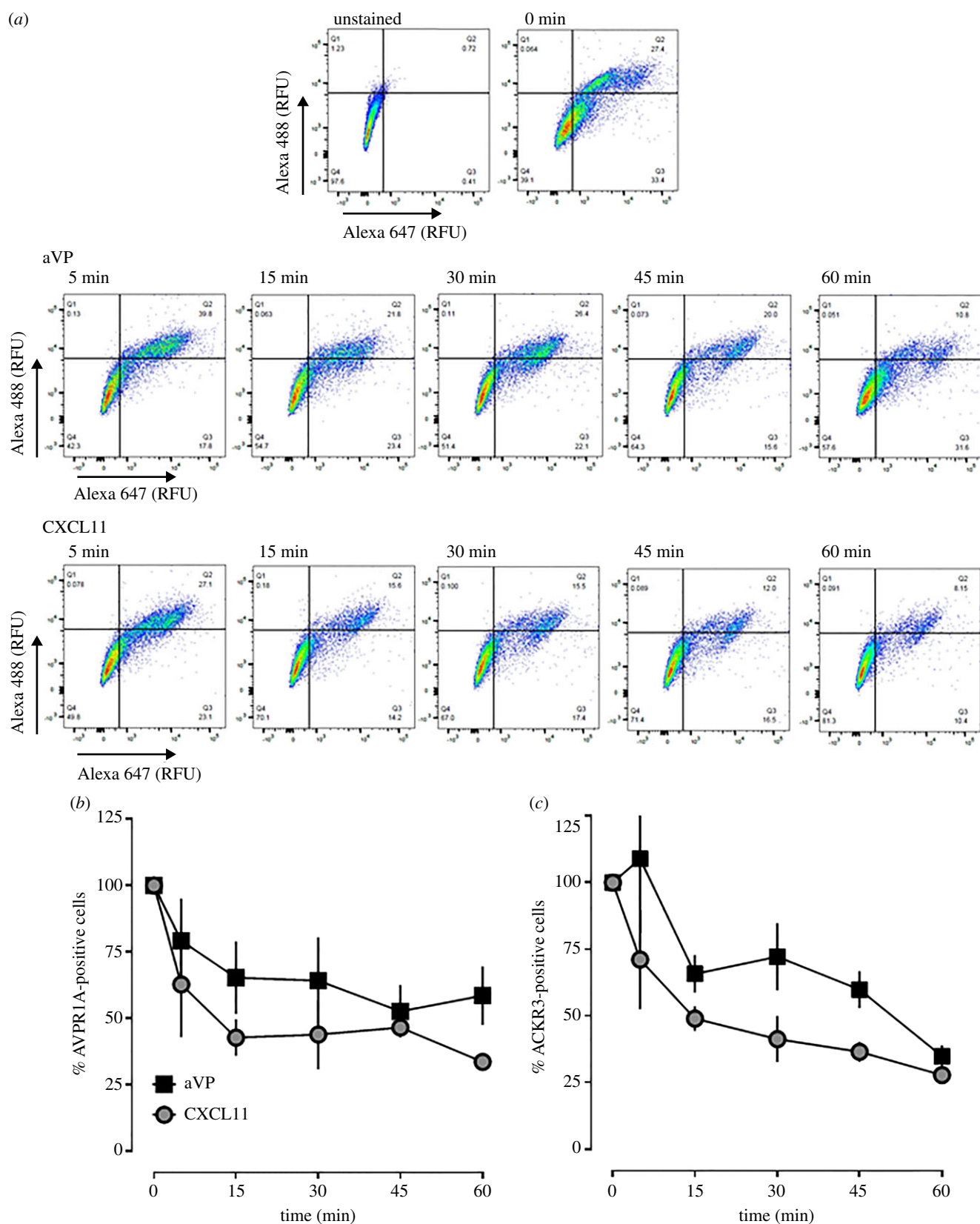


Figure 10. AVPR1A and ACKR3 co-internalize upon agonist stimulation in hVSMC. (a) hVSMCs were treated with $1 \mu\text{M}$ aVP or CXCL11 for up to 60 min, stained at 4°C with rabbit anti-AVPR1A/donkey anti-rabbit Alexa Fluor 647 and mouse anti-ACKR3/goat anti-mouse Alexa Fluor 488 and analysed for receptor expression via flow cytometry. RFU: relative fluorescence units. The horizontal and vertical lines show the gating thresholds for ACKR3 (Alexa 488) and AVPR1A (Alexa 647). (b) Quantification of AVPR1A-positive cells after incubation with aVP and CXCL11, as in (a). $n = 3$ independent experiments. (c) Quantification of ACKR3-positive cells after incubation with aVP and CXCL11, as in (a). $n = 3$ independent experiments.

changes the biochemical fingerprint of each receptor partner [52]. We currently cannot comment on the physiological consequences of AVPR1A:ACKR3 heteromerization on ACKR3-mediated effects on cell function due to the lack of

appropriate read-outs that are characteristic for ACKR3 and independent of CXCR4. Similarly, the possible roles of AVPR1A:CXCR4 heteromers, which occur after ACKR3 depletion, remain to be determined. Our findings, however,

indicate that AVPR1A:ACKR3 complexes are essential for AVPR1A function in vascular smooth muscle and suggest that ACKR3 activation within the heteromeric complex attenuates aVP-mediated vasoconstriction.

We have shown previously that hetero-oligomerization between $\alpha_{1B/D}$ -AR and the ACKR3:CXCR4 heteromer is essential for $\alpha_{1B/D}$ -AR function in vascular smooth muscle and that ACKR3 activation attenuates α_1 -AR-mediated vasoconstriction and $\alpha_{1B/D}$ -AR signalling in hVSMC [19–21]. In combination with the findings of the present study, these data support the concept that ACKR3 functions as a critical regulator vascular smooth muscle function: ACKR3 in the agonist-free conformation facilitates $G\alpha_q$ coupling of α_1 -AR and AVPR1A via direct physical interactions within the heteromeric complex. In the agonist-bound conformation, ACKR3 inhibits G protein coupling of the receptor partners and induces internalization of the heteromeric receptor complex.

Our findings provide a molecular mechanism for the previously described effects of synthetic ACKR3 ligands on blood pressure regulation in animals [4,7] and for interactions between the innate immune and vasoactive neurohormonal systems. This function of ACKR3 offers a mechanistic basis for the clinical observation that systemic levels of CXCL12, which preferentially acts as an ACKR3 agonist in VSMC [7], are significantly elevated in patients with sepsis and septic shock; the latter typically present with hypotension due to vasodilatory shock and vasopressor refractoriness [53–57]. In addition, significantly increased systemic CXCL11 concentrations have recently been described in patients with hypertension [58], which could reflect an adaptive response to reduce vascular resistance. Our findings provide another example for the functional relevance of GPCR heteromers and insights into the regulation and biological functions of ACKR3 and AVPR1A, which could facilitate the development of improved pharmacological strategies to modulate vascular function.

3. Material and methods

3.1. Proteins, peptides and reagents

PE and aVP were purchased from Sigma-Aldrich, ubiquitin was from R&D Systems, CXCL11 and CXCL12 were from Protein Foundry, and TC14012 was from Tocris Biosciences. CXCL11_{3–73} was purified as N-terminal His₆SUMO fusion proteins in *Escherichia coli* as previously described [7,59,60]. Cells were grown in Terrific Broth and induced with 1 mM isopropyl β -D-1-thiogalactopyranoside before being harvested and stored at -80°C . Cell pellets were lysed, and lysates were clarified by centrifugation (12 000g for 20 min). The supernatant and solubilized inclusion body pellets were loaded onto Ni-NTA resin and after 1 h proteins were eluted with 6 M guanidinium chloride, 50 mM Na₂PO₄ (pH 7.4), 300 mM NaCl, 500 mM imidazole, 0.2% sodium azide and 0.1% β -mercaptoethanol. The eluate was pooled and refolded via dilution overnight before cleavage of the His₆SUMO fusion tag and chemokine were separated using cation-exchange chromatography (SP Sepharose Fast Flow resin; GE Healthcare UK Ltd) and the eluate was subjected to reverse-phase high-performance liquid chromatography as a final purification. Proteins were frozen, lyophilized and stored at -20°C . Purification, folding and homogeneity of recombinant proteins

were verified by SDS-PAGE, MALDI-TOF spectroscopy and ¹H-¹⁵N HSQC NMR spectroscopy. The peptide analogues of transmembrane helix 2 (TM2; YILNLAIAADLWVLTIPV WVVDDD), TM4 (VVCILWLLAFCVSLPDTYYLDD) and TM7 (DDDLHVTQCLSLVHCCVNPVLYSFIN) of ACKR3 were as described previously [21].

3.2. Plasmids

The human AVPR1A cDNA sequence was from the AVPR1A-TANGO plasmid (Addgene, plasmid #66225). The hRLuc cDNA was PCR-amplified from pIRES-Myc-hCXCR4-Rluc, which was generously provided by Dr Michel Bouvier, with primers carrying the AgeI and XbaI sites at either end, respectively, and ligated with the C-terminus of AVPR1A at the corresponding sites. Human CXCR4 and ACKR3 cDNAs were from the CXCR4-TANGO (Addgene, plasmid #66262) and the ACKR3-TANGO (Addgene, plasmid #66265) plasmids. The EYFP cDNA was PCR-amplified from pEYFP with primers harbouring AgeI and XbaI sites and ligated with the C-terminus of ACKR3. All plasmids were confirmed by sequencing.

3.3. Cells

hVSMCs (primary aortic smooth muscle cells, ATCC PCS-100-012), A7r5 cells (ATCC-CRL-1444) and HEK293T cells (ATCC-CRL-11268) were purchased from American Type Culture Collection. hVSMCs were cultured in vascular basal media (ATCC PCS-100-030) supplemented with the vascular smooth muscle growth kit (ATCC PCS-100-042), containing 100 U ml⁻¹ penicillin and 100 $\mu\text{g ml}^{-1}$ streptomycin. hVSMCs were used between passages 2–5. HEK293T and A7r5 cells were cultured in high-glucose Dulbecco's Modified Eagle's Medium containing 10 mg ml⁻¹ sodium pyruvate, 2 mM L-glutamine, 10% (vol/vol) FBS, 1 \times non-essential amino acids, 100 U ml⁻¹ penicillin and 100 $\mu\text{g ml}^{-1}$ streptomycin. The HTLA cell line, a HEK293 cell line stably expressing a tTA-dependent luciferase reporter and a β -arrestin 2–TEV fusion gene [27] were generously provided by the laboratory of Dr Bryan Roth and maintained in high-glucose Dulbecco's Modified Eagle's Medium supplemented with 10% (vol/vol) FBS, 1 \times non-essential amino acids, 100 U ml⁻¹ penicillin, 100 $\mu\text{g ml}^{-1}$ streptomycin, 50 $\mu\text{g ml}^{-1}$ hygromycin B and 2 $\mu\text{g ml}^{-1}$ puromycin. All cells were cultured in a humidified environment at 37°C, 5% CO₂.

3.4. Proximity ligation assays

PLAs were performed as described in detail previously [19–21,61]. In brief, cells were grown and fixed on eight-well chamber slides (Nunc). Cells were fixed with 4% (wt/vol) paraformaldehyde for 15 min at room temperature and then blocked overnight at 4°C with 3% (wt/vol) BSA in PBS. To visualize individual proteins, slides were incubated with rabbit anti-HA (AbCam Ab9110), mouse anti-FLAG (Sigma-Aldrich F1804), rabbit anti-AVPR1A (Bioss BS-11598R), mouse anti-ACKR3 (R&D MAB42273), goat anti-CXCR4 (AbCam Ab1670) or mouse anti-phospho-MLC 2 (Ser19) (pMLC2, Cell Signaling Technology, 3675) at 37°C for 105 min in a humidifying chamber. To assess how permeabilization of the plasma membrane affects the PLA signals for pMLC2, cells were incubated in 0.5% Triton X-100 in PBS for 20 min at room temperature following fixation. To visualize receptor–receptor

interactions, slides were incubated with a combination of rabbit anti-HA (AbCam Ab9110) and mouse anti-FLAG (Sigma F1804), rabbit anti-AVPR1A (Bioss BS-11598R) and mouse anti-ACKR3 (R&D MAB42273) or goat anti-CXCR4 (AbCam Ab1670) at 37°C for 105 min in a humidifying chamber. All antibodies were used in dilutions of 1:500. Slides were then washed with PBS and incubated (60 min at 37°C in a humidifying chamber) with secondary species-specific antibodies conjugated with plus and minus Duolink II PLA probes (1:5), as appropriate. Negative control slides were incubated with omission of one primary antibody. Slides were washed again with PLA wash buffer A (Duolink II) and then incubated with ligation-ligase solution (30 min at 37°C in a humidifying chamber), and also washed with PLA wash buffer A and then incubated with amplification polymerase solution (100 min at 37°C in a humidifying chamber). Slides were then washed twice with PLA wash buffer B (Duolink II), once with 0.01× PLA wash buffer B and allowed to dry. Slides were then mounted with a minimal volume of Duolink II mounting medium with 4',6-diamidino-2-phenylindole dihydrochloride (DAPI) overnight, and PLA signals (Duolink In Situ Detection Reagent Red ($\lambda_{\text{excitation/emission}}$ 598/634 nm) were identified as fluorescent spots under a fluorescence microscope (Carl Zeiss Axiovert 200M with EC Plan-Neofluor objective lenses (40 × /1.30 oil) equipped with AXIO CAMMRC5 (Carl Zeiss) and AXIOVISION REL. 4.9.1 (Carl Zeiss) acquisition software) at room temperature. For each vision field 10 z-stack images in 1 µm sections were acquired and compressed. PLA signals were quantified using the Duolink IMAGE TOOL software (Sigma-Aldrich). Images were imported in merged.tiff formats containing both signal and nuclei channels. Merged images were visually verified for analytical quality. Comparisons and statistical analyses were performed only when PLA assays were performed on the same day in parallel experiments, and fluorescence microscopy was performed with the identical settings. For each experiment and condition, 10 randomly selected non-overlapping vision fields were analysed.

3.5. Deconvolution three-dimensional imaging

Deconvolution three-dimensional imaging was performed as described previously [19]. In brief, z-stack images were collected (from bottom to top, 20 sections of 0.5 µm) using identical acquisition parameters with a DeltaVision wide-field fluorescent microscope (Applied Precision, GE) equipped with a digital camera (CoolSNAP HQ; Photometrics), using a 1.4-numerical aperture 100× objective lens. Excitation light was generated using the Insight SSI solid-state illumination module (Applied Precision, GE), and images were deconvolved with the SOFTWoRx deconvolution software (Applied Precision, GE). Following deconvolution, images were quantified by IMARIS (Bitplane) software using the Surfaces feature function, generating surfaces around red puncta. Three-dimensional views of images were generated using the Surpass mode of IMARIS software.

3.6. Co-immunoprecipitation analyses of receptor interactions

Co-immunoprecipitation experiments with hVSMC and HEK293T cells were performed using the ThermoScientific Pierce co-immunoprecipitation kit (cat. no. 26149), as described

[21]. A total of 50 µg of rabbit anti-AVPR1A (Bioss BS-11598R), mouse anti-HA (Bioss bsm-50131M) or anti-rabbit IgG (AbCam Ab27478) were incubated with 50 µl of Amino Link Plus coupling resin for 180 min at room temperature. A cell lysate (1000 µg) was precleared with 50 µl of the control agarose resin slurry (60 min at 4°C). Immobilized anti-AVPR1A resin, anti-HA resin and anti-IgG resin were incubated with a pre-cleared lysate for 48 h at 4°C. After incubation, the resins were washed three times with 200 µl of IP lysis/wash buffer, once with conditioning buffer, and protein was eluted using 60 µl of elution buffer. Samples were analysed by western blotting.

3.7. Western blotting

Western blotting with rabbit anti-AVPR1A (Bioss BS-11598R), rabbit anti-ACKR3 (AbCam Ab38089), goat anti-CXCR4 (Abcam Ab1670), rabbit anti-β₂-AR (Abcam Ab36956), mouse anti-HA (Bioss bsm-50131M) or mouse anti-FLAG (Sigma-Aldrich F1804) in combination with anti-rabbit, anti-mouse (GE Healthcare) or anti-goat (Sigma-Aldrich) IgG horseradish peroxidase-linked whole antibody was performed as described previously [21].

3.8. Gene silencing via RNA interference

ACKR3 and CXCR4 siRNA gene silencing was performed as described previously [19,21,62]. In brief, cells were grown in 2 ml Accell siRNA delivery media per well (Dharmacon) in six-well plates (Nunc). Commercially available Accell ACKR3 and CXCR4 siRNA were reconstituted with 1× siRNA buffer to a stock concentration of 100 µM. Cells were then transfected with 1 µM ACKR3/CXCR4 siRNA and incubated for 72 h at 37°C, 5% CO₂. Accell NT-siRNA pool was used as a negative control. After 72 h, cells were assayed for receptor cell surface expression and used for signalling experiments.

3.9. GPCR gene transfections

HEK293T cells were transiently transfected with 1.5 µg of DNA encoding either HA-AVPR1A, FLAG-ACKR3 or FLAG-CXCR4 with a combination of two GPCR encoding DNAs, as indicated, using Lipofectamine 3000 (ThermoScientific) as per the manufacturer's protocol. All cDNAs were from the Addgene Tango plasmids subcloned in pcDNA3 with either HA- or FLAG-tag at the N-terminus. Empty vector, pcDNA3, was used as a control. Twenty-four hours later, cells were fixed on chamber slides for PLA or lysed for co-immunoprecipitation experiments.

3.10. Inositol trisphosphate enzyme-linked immunosorbent assay

IP₃ enzyme-linked immunosorbent assays were purchased from LS Bio and performed as per the manufacturer's protocol (LS BIO F10644). In brief, hVSMCs were grown to confluency in six-well dishes (Nunc) and then treated as described in the Results section. Cells were then washed once with cold PBS, 225 µl of cold PBS was added to each well and cells were lysed by ultrasonication. The cell lysate was centrifuged for 10 min at 4°C at 1500g to remove cellular debris. The total protein concentration in the supernatant was determined with the Bio-Rad DC Protein Assay as per the

manufacturer's protocol (Bio-Rad 500-0116). Equivalent amounts of total protein were added to the ELISA strips diluted in the provided sample diluent (1 : 5 and 1 : 10). The assay was then completed as per the manufacturer's protocol. Optical densities were read on a Biotek Synergy II microplate reader (absorbance at 450 nm), and IP₃ concentrations were extrapolated from the standard curve.

3.11. PRESTO-Tango β -arrestin recruitment assay

The PRESTO-Tango (parallel receptorome expression and screening via transcriptional output, with transcriptional activation following arrestin translocation) assay was performed as recently described [27]. The Tango plasmids were a gift from Dr Bryan Roth (all from Addgene). HTLA cells (2.5×10^5 per well) were seeded in a six-well plate and transfected with 1.5 μ g of the Tango plasmids using Lipofectamine 3000 (ThermoScientific). The following day, transfected HTLA cells (1×10^5 cells per well) were plated onto poly-L-lysine precoated 96-well microplates and allowed to attach to the plate surface for at least 4 h prior to treatment. Proteins used for treatment were prepared in twice the final concentration in culture media, added at a 1 : 1 vol/vol ratio and incubated overnight at 37°C, 5% CO₂ in a humidified environment. The following morning, media were removed from cell culture plates and replaced with a 100 μ l 1 : 5 mixture of Bright-Glo (Promega) and 1 \times HBSS, 20 mM HEPES solution. Plates were then incubated at room temperature before measuring luminescence on a Biotek Synergy II plate reader.

3.12. Intermolecular bioluminescence resonance energy transfer assay

HEK293T cells were seeded in 12-well plates and transfected with AVPR1A-hRluc alone or together with plasmids encoding EYFP or ACKR3-EYFP using the Lipofectamine 3000 transfection reagent (ThermoScientific). For BRET titration assays, AVPR1A-hRluc at the fixed amount of 50 ng was co-transfected with increasing amounts of EYFP or ACKR3-EYFP. For BRET assays at a constant acceptor : donor ratio, increasing amounts of AVPR1A-hRluc and ACKR3-EYFP were co-transfected at a ratio of 1 : 10. In all assays, empty vector pcDNA3 was added to maintain the total cDNA amount for each transfection reaction constant. After an overnight incubation, cells were seeded in poly-L-lysine coated 96-well white plates and incubated again overnight. Cells were then washed with PBS and fluorescence was measured in a Biotek Synergy II plate reader ($\lambda_{\text{excitation}}$ 485 nm, $\lambda_{\text{emission}}$ 528 nm). For BRET measurements, coelenterazine H (Nanolight Technology) at 5 μ M in PBS was added to the cells. After 10 min incubation at room temperature, luminescence was measured at 460 ± 40 and 528 ± 20 nm. The BRET signal is calculated as the ratio of RLU measured at 528 \pm 20 nm over RLU at 460 \pm 40 nm. The net BRET is calculated by subtracting the BRET signal detected when the AVPR1A-hRluc was transfected alone. For titration experiments, net BRET ratios are expressed as a function of EYFP/total luminescence.

3.13. Receptor internalization assay

Assessment of receptor internalization upon agonist stimulation was achieved via flow cytometry. hVSMCs were treated

with 1 μ M of aVP or CXCL11 for various time points. The cells were washed once with ice cold DPBS, blocked and stained with rabbit anti-AVPR1A (Bioss BS-11598R) and mouse anti-ACKR3 (R&D MAB42273) antibodies at 1 : 200 dilution for 1 h on ice. Cells were then washed twice with FACS wash buffer (1 \times PBS, 2% FBS and 0.01% NaN₃), and secondary antibodies were added at a 1 : 500 dilution and incubated for 30 min on ice (donkey anti-rabbit Alexa Fluor 647, Invitrogen A-31573 and donkey anti-mouse Alexa Fluor 488, Invitrogen A-21202). Cells were washed twice with FACS wash buffer and then fixed with 4% paraformaldehyde at room temperature for 15 min. After two additional washes, the cells were counted on a BD FACS Canto II (BD Biosciences) flow cytometer. The fluorescence intensities of at least 3×10^4 cells were recorded and analysed using the FlowJo software (Tree Star).

3.14. Flow cytometry

Flow cytometry was used to assess equivalent recombinant Tango receptor expression. HTLA cells were labelled with rabbit anti-FLAG-Alexa Fluor 647 (R&D Systems IC8529R). The fluorescence intensities of at least 3×10^4 cells were recorded and analysed using the FlowJo software (Tree Star).

3.15. Pressure myography

Pressure myography was performed as described in detail previously with slight modifications [7,63]. Male Sprague-Dawley rats (Harlan) were anaesthetized with 3.5% isoflurane. The mesentery was immediately removed and placed in 130 mM NaCl, 4.7 mM KCl, 1.18 mM KH₂PO₄, 1.17 mM MgSO₄, 14.9 mM NaHCO₃, 5.5 mM D-glucose, 0.026 mM EDTA and 1.16 mM CaCl₂ aerated with 95% O₂, 5% CO₂ at 37°C. The animal was then euthanized by cardiectomy and bilateral decompression of the lungs. Third- or fourth-order mesenteric arteries were dissected free from the mesentery, mounted onto two glass cannulae with United States Pharmacopeia (USP) scale 11-0 sutures and pressurized to 80 mmHg in a DMT 110P pressure myograph system (DMT-USA). The intraluminal solution and the vessel bath solution were the same as described before. The vessel bath solution was continuously aerated with 95% O₂, 5% CO₂ throughout the experiment. The outer diameter (o.d.) of the pressurized vessel was then continuously measured and recorded via digital video-edge detection upon the addition of increasing doses of PE or aVP to the vessel bath.

3.16. Data analyses

Data are expressed as mean \pm standard error of the mean from *n* independent experiments that were performed on different days. Data were analysed using GRAPHPAD PRISM v. 7 software. Unpaired Student's *t*-test or one-way analyses of variance (ANOVA) with Dunnett's multiple comparison post hoc test for multiple comparisons were used, as appropriate. Dose-response curves were analysed using nonlinear regression analyses. A two-tailed *p* < 0.05 was considered significant.

Ethics. All procedures involving animals were conducted in accordance with the Guide for the Care and Use of Laboratory Animals, 8th edition and were approved by the Institutional Animal Care and Use Committee of Loyola University Chicago (no. 205102, 10 July 2013).

Data accessibility. All plasmids are available from Addgene (<http://www.addgene.org/>). The original datasets generated and analysed during this study are available from the corresponding author on reasonable request.

Authors' contributions. L.J.A., H.M.L., X.G., J.M.E. and Y.-H.C. developed methods and performed experiments. L.J.A. and M.M. conceived and designed experiments. L.J.A., H.M.L., X.G., J.M.E. and M.M. analysed data. A.M.N., B.F.V. and V.G. provided

reagents. M.M. and L.J.A. wrote the manuscript. All authors reviewed and commented on the manuscript and approved the final version.

Competing interests. We declare we have no competing interests.

Funding. This work was supported by the National Institute of General Medical Sciences (award R01GM107495) and by the National Cancer Institute (award R01CA188427). The content is solely the responsibility of the authors.

References

- Gambaryan N, Perros F, Montani D, Cohen-Kaminsky S, Mazmanian M, Renaud JF, Simonneau G, Lombet A, Humbert M. 2011 Targeting of c-kit+ haematopoietic progenitor cells prevents hypoxic pulmonary hypertension. *Eur. Respir. J.* **37**, 1392–1399. (doi:10.1183/09031936.00045710)
- Yu L, Hales CA. 2011 Effect of chemokine receptor CXCR4 on hypoxia-induced pulmonary hypertension and vascular remodeling in rats. *Respir. Res.* **12**, 21. (doi:10.1186/1465-9921-12-21)
- Chu PY, Zatta A, Kiriazis H, Chin-Dusting J, Du XJ, Marshall T, Kaye DM. 2011 CXCR4 antagonism attenuates the cardiorenal consequences of mineralocorticoid excess. *Circ. Heart Fail.* **4**, 651–658. (doi:10.1161/CIRCHEARTFAILURE.110.960831)
- Sartina E *et al.* 2012 Antagonism of CXCR7 attenuates chronic hypoxia-induced pulmonary hypertension. *Pediatr. Res.* **71**, 682–688. (doi:10.1038/pr.2012.30)
- Bach HH, Wong YM, LaPorte HM, Gamelli RL, Majetschak M. 2016 Pharmacological targeting of chemokine (C-X-C motif) receptor 4 in porcine polytrauma and hemorrhage models. *J. Trauma Acute Care Surg.* **80**, 102–110. (doi:10.1097/TA.0000000000000865)
- Farkas D, Kraskauskas D, Drake JI, Alhussaini AA, Kraskauskienė V, Bogaard HJ, Cool CD, Voelkel NF, Farkas L. 2014 CXCR4 inhibition ameliorates severe obliterative pulmonary hypertension and accumulation of C-kit(+) cells in rats. *PLoS ONE* **9**, e89810. (doi:10.1371/journal.pone.0089810)
- Bach HH, Wong YM, Tripathi A, Nevins AM, Gamelli RL, Volkman BF, Byron KL, Majetschak M. 2014 Chemokine (C-X-C motif) receptor 4 and atypical chemokine receptor 3 regulate vascular alpha(1)-adrenergic receptor function. *Mol. Med.* **20**, 435–447. (doi:10.2119/molmed.2014.00101)
- Bachelier F *et al.* 2014 International union of pharmacology. LXXXIX. Update on the extended family of chemokine receptors and introducing a new nomenclature for atypical chemokine receptors. *Pharmacol. Rev.* **66**, 1–79. (doi:10.1124/pr.113.007724)
- Rajagopal S, Kim J, Ahn S, Craig S, Lam CM, Gerard NP, Gerard C, Lefkowitz RJ. 2010 Beta-arrestin- but not G protein-mediated signaling by the 'decoy' receptor CXCR7. *Proc. Natl Acad. Sci. USA* **107**, 628–632. (doi:10.1073/pnas.0912852107)
- Levoye A, Balabanian K, Baleux F, Bachelier F, Lagane B. 2009 CXCR7 heterodimerizes with CXCR4 and regulates CXCL12-mediated G protein signaling. *Blood* **113**, 6085–6093. (doi:10.1182/blood-2008-12-196618)
- Decailot FM, Kazmi MA, Lin Y, Ray-Saha S, Sakmar TP, Sachdev P. 2011 CXCR7/CXCR4 heterodimer constitutively recruits beta-arrestin to enhance cell migration. *J. Biol. Chem.* **286**, 32 188–32 197. (doi:10.1074/jbc.M111.277038)
- Watts AO *et al.* 2013 Identification and profiling of CXCR3–CXCR4 chemokine receptor heteromer complexes. *Br. J. Pharmacol.* **168**, 1662–1674. (doi:10.1111/bph.12064)
- Sohy D, Yano H, de Nadai P, Urizar E, Guillabert A, Javitch JA, Parmentier M, Springael JY. 2009 Hetero-oligomerization of CCR2, CCR5, and CXCR4 and the protean effects of 'selective' antagonists. *J. Biol. Chem.* **284**, 31 270–31 279. (doi:10.1074/jbc.M109.054809)
- LaRocca TJ *et al.* 2010 beta2-Adrenergic receptor signaling in the cardiac myocyte is modulated by interactions with CXCR4. *J. Cardiovasc. Pharmacol.* **56**, 548–559. (doi:10.1097/FJC.0b013e3181f713fe)
- de Poorter C, Baertsoen K, Lannoy V, Parmentier M, Springael JY. 2013 Consequences of ChemR23 heteromerization with the chemokine receptors CXCR4 and CCR7. *PLoS ONE* **8**, e58075. (doi:10.1371/journal.pone.0058075)
- Sohy D, Parmentier M, Springael JY. 2007 Allosteric transinhibition by specific antagonists in CCR2/CXCR4 heterodimers. *J. Biol. Chem.* **282**, 30 062–30 069. (doi:10.1074/jbc.M705302200)
- Pello OM *et al.* 2008 Ligand stabilization of CXCR4/delta-opioid receptor heterodimers reveals a mechanism for immune response regulation. *Eur. J. Immunol.* **38**, 537–549. (doi:10.1002/eji.200737630)
- Coke CJ, Scarlett KA, Chetram MA, Jones KJ, Sandifer BJ, Davis AS, Marcus AI, Hinton CV. 2016 Simultaneous activation of induced heterodimerization between CXCR4 chemokine receptor and cannabinoid receptor 2 (CB2) reveals a mechanism for regulation of tumor progression. *J. Biol. Chem.* **291**, 9991–10005. (doi:10.1074/jbc.M115.712661)
- Tripathi A, Vana PG, Chavan TS, Brueggemann LI, Byron KL, Tarasova NI, Volkman BF, Gaponenko V, Majetschak M. 2015 Heteromerization of chemokine (C-X-C motif) receptor 4 with alpha1A/B-adrenergic receptors controls alpha1-adrenergic receptor function. *Proc. Natl Acad. Sci. USA* **112**, E1659–E1668. (doi:10.1073/pnas.1417564112)
- Evans AE *et al.* 2016 New insights into mechanisms and functions of chemokine (C-X-C Motif) receptor 4 heteromerization in vascular smooth muscle. *Int. J. Mol. Sci.* **17**, E971. (doi:10.3390/ijms17060971)
- Albee LJ, Eby JM, Tripathi A, Laporte HM, Gao X, Volkman BF, Gaponenko V, Majetschak M. 2017 alpha-1-Adrenoceptors function within hetero-oligomeric complexes with chemokine receptors ACKR3 and CXCR4 in vascular smooth muscle cells. *J. Am. Heart Assoc.* **6**, e006575. (doi:10.1161/JAHA.117.006575)
- Wei SG, Zhang ZH, Yu Y, Weiss RM, Felder RB. 2012 Central actions of the chemokine stromal cell-derived factor 1 contribute to neurohumoral excitation in heart failure rats. *Hypertension* **59**, 991–998. (doi:10.1161/HYPERTENSIONAHA.111.188086)
- Callewaere C, Banisadr G, Desarmenien MG, Mechighel P, Kitabgi P, Rostene WH, Melik Parsadaniantz S. 2006 The chemokine SDF-1/CXCL12 modulates the firing pattern of vasopressin neurons and counteracts induced vasopressin release through CXCR4. *Proc. Natl Acad. Sci. USA* **103**, 8221–8226. (doi:10.1073/pnas.0602620103)
- Saini V, Staren DM, Ziarek JJ, Nashaat ZN, Campbell EM, Volkman BF, Marchese A, Majetschak M. 2011 The CXC chemokine receptor 4 ligands ubiquitin and stromal cell-derived factor-1alpha function through distinct receptor interactions. *J. Biol. Chem.* **286**, 33 466–33 477. (doi:10.1074/jbc.M111.233742)
- Proost P *et al.* 2007 Proteolytic processing of CXCL11 by CD13/aminopeptidase N impairs CXCR3 and CXCR7 binding and signaling and reduces lymphocyte and endothelial cell migration. *Blood* **110**, 37–44. (doi:10.1182/blood-2006-10-049072)
- Proost P *et al.* 2001 Amino-terminal truncation of CXCR3 agonists impairs receptor signaling and lymphocyte chemotaxis, while preserving antiangiogenic properties. *Blood* **98**, 3554–3561.
- Kroeze WK, Sassano MF, Huang XP, Lansu K, McCorvy JD, Giguere PM, Sciaky N, Roth BL. 2015 PRESTO-Tango as an open-source resource for interrogation of the druggable human GPCRome. *Nat. Struct. Mol. Biol.* **22**, 362–369. (doi:10.1038/nsmb.3014)
- Eby JM, Abdelkarim H, Albee LJ, Tripathi A, Gao X, Volkman BF, Gaponenko V, Majetschak M. 2017 Functional and structural consequences of chemokine (C-X-C motif) receptor 4 activation with cognate and non-cognate agonists. *Mol. Cell*

- Biochem.* **434**, 143–151. (doi:10.1007/s11010-017-3044-7)
29. Burns JM *et al.* 2006 A novel chemokine receptor for SDF-1 and I-TAC involved in cell survival, cell adhesion, and tumor development. *J. Exp. Med.* **203**, 2201–2213. (doi:10.1084/jem.20052144)
 30. Benredjem B, Girard M, Rhainds D, St-Onge G, Heveker N. 2017 Mutational analysis of atypical chemokine receptor 3 (ACKR3/CXCR7) interaction with its chemokine ligands CXCL11 and CXCL12. *J. Biol. Chem.* **292**, 31–42. (doi:10.1074/jbc.M116.762252)
 31. Gifford AN, Bruneus M, Gatley SJ, Lan R, Makriyannis A, Volkow ND. 1999 Large receptor reserve for cannabinoid actions in the central nervous system. *J. Pharmacol. Exp. Ther.* **288**, 478–483.
 32. Ethier MF, Schaefer OP, Samant N, Yamaguchi H, Madison JM. 1996 Muscarinic receptor reserve for inhibition of cAMP accumulation in bovine trachealis cells. *Am. J. Physiol.* **270**, L199–L207.
 33. Gravel S, Malouf C, Boulais PE, Berchiche YA, Oishi S, Fujii N, Leduc R, Sinnott D, Heveker N. 2010 The peptidomimetic CXCR4 antagonist TC14012 recruits beta-arrestin to CXCR7: roles of receptor domains. *J. Biol. Chem.* **285**, 37 939–37 943. (doi:10.1074/jbc.C110.147470)
 34. Russell JA. 2011 Bench-to-bedside review: vasopressin in the management of septic shock. *Crit. Care* **15**, 226. (doi:10.1186/cc8224)
 35. Soderberg O *et al.* 2006 Direct observation of individual endogenous protein complexes in situ by proximity ligation. *Nat. Methods* **3**, 995–1000. (doi:10.1038/nmeth947)
 36. Marullo S, Bouvier M. 2007 Resonance energy transfer approaches in molecular pharmacology and beyond. *Trends Pharmacol. Sci.* **28**, 362–365. (doi:10.1016/j.tips.2007.06.007)
 37. Tripathi A, Gaponenko V, Majetschak M. 2015 Commercially available antibodies directed against alpha-adrenergic receptor subtypes and other G protein-coupled receptors with acceptable selectivity in flow cytometry experiments. *Naunyn Schmiedebergs Arch. Pharmacol.* **389**, 243–248. (doi:10.1007/s00210-015-1196-0)
 38. Isberg V *et al.* 2017 GPCRdb: an information system for G protein-coupled receptors. *Nucleic Acids Res.* **45**, 2936. (doi:10.1093/nar/gkw1218)
 39. Kasai RS, Suzuki KG, Prossnitz ER, Koyama-Honda I, Nakada C, Fujiwara TK, Kusumi A. 2011 Full characterization of GPCR monomer-dimer dynamic equilibrium by single molecule imaging. *J. Cell Biol.* **192**, 463–480. (doi:10.1083/jcb.201009128)
 40. Cai X, Bai B, Zhang R, Wang C, Chen J. 2017 Apelin receptor homodimer-oligomers revealed by single-molecule imaging and novel G protein-dependent signaling. *Sci. Rep.* **7**, 40335. (doi:10.1038/srep40335)
 41. Hern JA, Baig AH, Mashanov GI, Birdsall B, Corrie JE, Lazareno S, Molloy JE, Birdsall NJ. 2010 Formation and dissociation of M1 muscarinic receptor dimers seen by total internal reflection fluorescence imaging of single molecules. *Proc. Natl Acad. Sci. USA* **107**, 2693–2698. (doi:10.1073/pnas.0907915107)
 42. Tarasov SG *et al.* 2011 Structural plasticity of a transmembrane peptide allows self-assembly into biologically active nanoparticles. *Proc. Natl Acad. Sci. USA* **108**, 9798–9803. (doi:10.1073/pnas.1014598108)
 43. Tarasova NI, Rice WG, Michejda CJ. 1999 Inhibition of G-protein-coupled receptor function by disruption of transmembrane domain interactions. *J. Biol. Chem.* **274**, 34 911–34 915.
 44. Hebert TE, Moffett S, Morello JP, Loisel TP, Bichet DG, Barret C, Bouvier M. 1996 A peptide derived from a beta2-adrenergic receptor transmembrane domain inhibits both receptor dimerization and activation. *J. Biol. Chem.* **271**, 16 384–16 392.
 45. Pfeiffer M, Kirscht S, Stumm R, Koch T, Wu D, Laugsch M, Schroder H, Holt V, Schulz S. 2003 Heterodimerization of substance P and mu-opioid receptors regulates receptor trafficking and resensitization. *J. Biol. Chem.* **278**, 51 630–51 637. (doi:10.1074/jbc.M307095200)
 46. Ferre S, Casado V, Devi LA, Filizola M, Jockers R, Lohse MJ, Milligan G, Pin JP, Guitart X. 2014 G protein-coupled receptor oligomerization revisited: functional and pharmacological perspectives. *Pharmacol. Rev.* **66**, 413–434. (doi:10.1124/pr.113.008052)
 47. Martinez-Pinilla E, Rodriguez-Perez AI, Navarro G, Aguinaga D, Moreno E, Lanciego JL, Labandeira-Garcia JL, Franco R. 2015 Dopamine D2 and angiotensin II type 1 receptors form functional heteromers in rat striatum. *Biochem. Pharmacol.* **96**, 131–142. (doi:10.1016/j.bcp.2015.05.006)
 48. Goupil E *et al.* 2015 Angiotensin II type I and prostaglandin F2alpha receptors cooperatively modulate signaling in vascular smooth muscle cells. *J. Biol. Chem.* **290**, 3137–3148. (doi:10.1074/jbc.M114.631119)
 49. Terrillon S, Barberis C, Bouvier M. 2004 Heterodimerization of V1a and V2 vasopressin receptors determines the interaction with beta-arrestin and their trafficking patterns. *Proc. Natl Acad. Sci. USA* **101**, 1548–1553. (doi:10.1073/pnas.0305322101)
 50. Luker KE, Steele JM, Mihalko LA, Ray P, Luker GD. 2010 Constitutive and chemokine-dependent internalization and recycling of CXCR7 in breast cancer cells to degrade chemokine ligands. *Oncogene* **29**, 4599–4610. (doi:10.1038/onc.2010.212)
 51. Gomes I, Ayoub MA, Fujita W, Jaeger WC, Pfleger KD, Devi LA. 2016 G protein-coupled receptor heteromers. *Annu. Rev. Pharmacol. Toxicol.* **56**, 403–425. (doi:10.1146/annurev-pharmtox-011613-135952)
 52. Ferre S *et al.* 2009 Building a new conceptual framework for receptor heteromers. *Nat. Chem. Biol.* **5**, 131–134. (doi:10.1038/nchembio0309-131)
 53. Lesur O, Roussy JF, Chagnon F, Gallo-Payet N, Dumaine R, Sarret P, Chraïbi A, Chouinard L, Hogue B. 2010 Proven infection-related sepsis induces a differential stress response early after ICU admission. *Crit. Care* **14**, R131. (doi:10.1186/cc9102)
 54. Franchini S, Marciano T, Sorlini C, Campochiaro C, Tresoldi M, Sabbadini MG, Dagna L. 2015 Serum CXCL12 levels on hospital admission predict mortality in patients with severe sepsis/septic shock. *Am. J. Emerg. Med.* **33**, 1802–1804. (doi:10.1016/j.ajem.2015.08.047)
 55. Tunc T *et al.* 2015 Diagnostic value of elevated CXCR4 and CXCL12 in neonatal sepsis. *J. Matern. Fetal Neonatal Med.* **28**, 356–361. (doi:10.3109/14767058.2014.916683)
 56. Russell JA. 2006 Management of sepsis. *N. Engl. J. Med.* **355**, 1699–1713. (doi:10.1056/NEJMra043632)
 57. Chernow B, Rainey TG, Lake CR. 1982 Endogenous and exogenous catecholamines in critical care medicine. *Crit. Care Med.* **10**, 409–416.
 58. Altara R, Gu YM, Struijker-Boudier HA, Thijs L, Staessen JA, Blankesteyn WM. 2015 Left ventricular dysfunction and CXCR3 ligands in hypertension: from animal experiments to a population-based pilot study. *PLoS ONE* **10**, e0141394. (doi:10.1371/journal.pone.0141394)
 59. Takekoshi T, Ziarek JJ, Volkman BF, Hwang ST. 2012 A locked, dimeric CXCL12 variant effectively inhibits pulmonary metastasis of CXCR4-expressing melanoma cells due to enhanced serum stability. *Mol. Cancer Ther.* **11**, 2516–2525.
 60. Veldkamp CT, Seibert C, Peterson FC, De la Cruz NB, Haugner III JC, Basnet H, Sakmar TP, Volkman BF. 2008 Structural basis of CXCR4 sulfotyrosine recognition by the chemokine SDF-1/CXCL12. *Sci. Signal.* **1**, ra4.
 61. Tripathi A, Davis JD, Staren DM, Volkman BF, Majetschak M. 2014 CXC chemokine receptor 4 signaling upon co-activation with stromal cell-derived factor-1alpha and ubiquitin. *Cytokine* **65**, 121–125. (doi:10.1016/j.cyt.2013.12.008)
 62. Saini V, Marchese A, Majetschak M. 2010 CXC chemokine receptor 4 is a cell surface receptor for extracellular ubiquitin. *J. Biol. Chem.* **285**, 15 566–15 576. (doi:10.1074/jbc.M110.103408)
 63. Evans AE, Vana PG, Laporte HM, Kennedy RH, Gamelli RL, Majetschak M. 2016 Cardiovascular responsiveness to vasopressin and α 1-adrenergic receptor agonists after burn injury. *J. Burn Care Res.* **38**, 90–98. (doi:10.1097/BCR.0000000000000374)